Modeling the Stepping Mechanism of Development of Negative Lightning Leader

Artem Syssoev[1,2], Dmitry Iudin[1,2,3,*], Stanislav Davydenko[1,2], Vladimir Rakov[4]

1. Institute of Applied Physics of the Russian Academy of Sciences, Nizhny Novgorod, Russia
2. Space Research Institute of Russian Academy of Science, Moscow, Russia
3. Federal State Budgetary Educational Institution of Higher Education "Nizhny Novgorod State University of Architecture and Civil Engineering", Nizhny Novgorod, Russia
4. University of Florida, Gainesville, Florida, USA

ABSTRACT: Since 1930s, when Shonland has started his famous observations of the negative leader propagation, it has been discovered that they develop in a stepwise manner using a mechanism of the so-called space leaders in contrary to positive ones, which propagate continuously. Despite this fact has been known for about a hundred years, till now no one had developed any plausible model explaining this asymmetry. In this study we suggest a model of the stepped negative lightning leader development which for the first time allows carrying out the numerical simulation of its evolution. The model is based on the probability approach and the description of the discharge channels temporal evolution. One of the key features of our model is accounting of the presence of space streamers/leaders which play a key role in the process of a negative leader step formation. Their appearance becomes possible due to the accounting of potential influence of the space charge injected into the discharge gap by the negative leader streamer corona. The model takes into account an asymmetry between properties of negative and positive streamers which is based on the well-known from numerous laboratory measurements fact that positive streamers need about twice weaker electric field to appear and propagate as compared to negative ones. An extinction of a conducting channel as a possible way of its evolution is also assumed. This allows us to describe the sheath formation of leader channel. To verify the morphology and characteristics of the model discharge, we use the results of the high-speed video observations of natural negative stepped leaders. We can conclude that the key properties of model and natural negative leaders are very similar.

INTRODUCTION

Since the 1930s, when Schonland and his co-workers have started their pioneering optical observations of negative leader development (see, for example, *Rakov and Uman* [2003, ch. 4] and references therein), it has been known that negative leaders in virgin air always develop in a stepped manner, with the step length being of the order of tens of meters and interstep intervals of

---

the order of tens of microseconds. The Schonland's results are based on streak-camera records. More recent observations with framing cameras yielded shorter step lengths and shorter interstep intervals. In contrast, positive leaders usually develop continuously. Significant progress has been made lately in understanding the step-formation process using framing-camera records of rocket-triggered [*Gamerota et al.*, 2014] and natural [*Hill et al*, 2011; *Petersen and Beasley*, 2013; *Tran et al.*, 2014; *Lu et al*, 2016; *Qi et al*, 2016; *Jiang et al.*, 2017] lightning. The mechanism of step-formation process in lightning appears to be similar to that observed in long negative sparks [*Gorin and Shkilev*, 1976; *Ortega et al.*, 1994; *Rees et al.*, 1995]. However, many details of the step-formation process remain unclear, including the genesis and evolution of the space stem, connection of the space leader to the primary leader channel, and generation of negative corona streamer burst. As far as we know, to date, there are only two one-dimensional models of stepped-leader development considering the processes in its streamer zone, which lead to the formation of steps. The first one, developed by *Cooray and Arevalo* [2017], is devoted to the estimation of step length, step formation time, and propagation speed of stepped leaders as a function of the prospective return-stroke peak current. The second model of *Zhang et al.* [2017] is used to study the dynamics of branching of negative downward lightning leaders.

A better understanding of stepped leader propagation from the cloud to ground or to the grounded object is needed for improving lightning protection schemes. Further, the lightning return-stroke current largely depends on the charge distribution in the channel corona sheath. The corona-sheath charge may originate from the streamer zone developing from the leader tip and from the radial corona from the lateral leader channel surface, the relative contributions from these two sources being presently unknown. Formation of the leader channel corona sheath is an intrinsic process in our model, although only one of its sources (streamer zone at the leader tip) is considered.

In this study, we use a numerical model with unprecedentedly small grid spacing of 3 m. For comparison, the finest spatial resolution in numerical models of lightning discharges [*Iudin and Davydenko*, 2015; *Davydenko and Iudin*, 2016] was 10 m, and the typical values are 12.5-500 m [*Tan et al.*, 2006; *Riousset et al.*, 2007; *Mansell et al.*, 2010; *Iudin et al.*, 2015, 2017; *Wang et al.*, 2016]. Such a high spatial resolution is needed in modeling the negative-leader step formation process because the length of the negative-leader streamer zone [*Rakov and Uman*, 2003, p. 134-135], as well as the length of leader steps [*Hill et al.*, 2011; *Qi et al.*, 2016; *Jiang et al.*, 2017], can be of the order of 10 m or less. As far as we know, only a few numerical models [e.g., *Iudin and Davydenko*, 2015; *Davydenko and Iudin*, 2016; *Iudin et al.*, 2017] reproduce temporal evolution of discharge-channel properties. Moreover, many of the numerical models [e.g., *Tan et al.*, 2006; *Mansell et al.*, 2010]) don't include physical timing. In this study, the temporal evolution of discharge-channel properties allows us to consider, for the first time, the process of streamer-to-leader transition. The occurrence of steps in our model is possible only in the case of asymmetry between the initiation and propagation fields of positive and negative streamers. To the best of our knowledge, this widely known (see Appendix A) asymmetry has not been implemented in previous models.
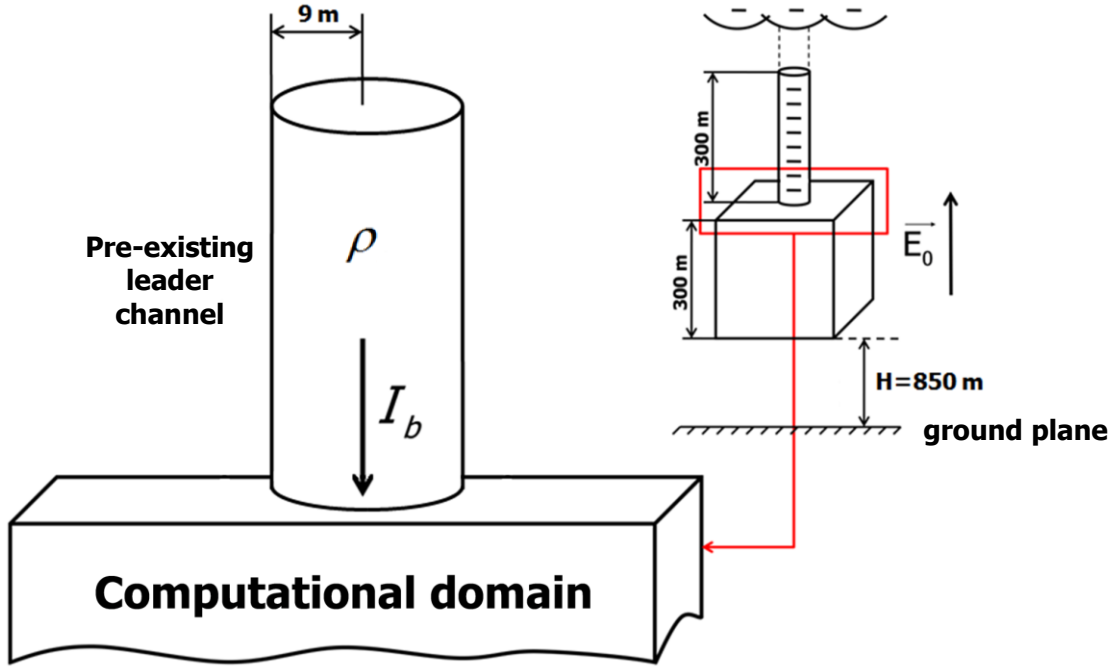
We compare the results of our simulations with high-speed optical records of lightning [*Hill et al.*, 2011; *Petersen and Beasley*, 2013; *Tran et al.*, 2014; *Lu et al.*, 2016; *Qi et al.*, 2016; *Jiang et al.*, 2017] and sparks [*Gorin and Shkilev*, 1976; *Ortega et al.*, 1994; *Rees et al.*, 1995], which are considered most informative to date.

MODEL FORMULATION

1) General configuration

Morphology and development of stepped leader in negative lightning are modeled in the Cartesian space region having the shape of a cube with an edge of 300 m. This cubical volume is divided into 10^6 identical cells, so that the spatial resolution (grid spacing) of our model is equal to 3 m. The center of the cubical computational domain is located at a height of 1 km above the ground level. A vertical uniformly-charged cylinder whose length is 300 m and radius is 9 m is attached to the top of the computational domain, as shown in Fig. 1. This cylinder simulates the previously created leader channel, whose lower end just arrived at the top of the computational domain. Thus, what we simulate in the present study is only the lower end of the descending negative leader. The background potential distribution is determined by (1) a constant, upward-directed electrical field E_0 produced by cloud charges and (2) negative charges deposited on the previously created channel. Image charges (due to the presence of ground) also contribute to the potential distribution. Figure 2 shows all possible directions of discharge extension.

The bulk of the pre-existing leader channel charge is assumed to reside in the corona sheath whose radius is expected to be of the order of meters or more, which is much larger than the millimeter-scale radius of the channel core [*Rakov and Uman*, 2003, p. 134-135]. The line charge density ρ of the pre-existing channel is set to 800 µC/m. The line charge on the cylinder axis is 132 µC/m and it is assumed to decrease as inverse radial distance *r* from the axis (the presence of channel core is neglected), which corresponds to the assumption of constant radial electric field in the corona sheath [*Bazelyan and Raizer*, 2000, p. 69]. The magnitude E_0 of the electric field produced by cloud charges (and their images) is assumed to be 30 kV/m, which is expected at an altitude of 1 km above ground level [*MacGorman and Rust*, 1998, p. 53]. Feeding current I_b (where "b" stands for the upper boundary of computational domain) is used to supply negative charge to the developing leader channel inside the computational domain. This current rapidly rises from zero to its maximum (steady-state) value. We used three maximum values (rounded to two significant digits) of I_b, 100, 210, and 350 A (the actual values were 104, 214, and 347 A, respectively). Current I_b is assumed to flow along the z-axis and be decoupled from the background charge density distribution within the cylinder.

Figure 1. Cubical computational domain placed 850 m above ground level and the simulated pre-existing leader channel attached to its top (not to scale). E_0 is the electric field produced by cloud charges and their images, representing induced charges on the ground surface. The pre-existing channel is negatively charged. Both cloud charges and pre-existing channel charges contribute to the background potential distribution inside the computational domain. ρ is the line charge density of the pre-existing leader channel, and I_b is the steady feeding current supplying negative charge to the leader channel developing inside the computational domain. In this study, ρ and I_b are assumed to be decoupled.

2) Electric potential and electric field distributions

Electrical potential φ produced by both constant electric field E_0 and charges (and their images) located both at the grid nodes of the computational domain and outside the computational domain can be calculated as the solution of Poisson's equation. In this study, the potential is calculated using the following relation:

$$\varphi\left(\vec{r}\right)=\frac{1}{4\pi\varepsilon_0}\left(\sum_{r'\neq r}\left\{\frac{q_{\vec{r'}}}{\left|\vec{r}-\vec{r'}\right|}-\frac{q_{\vec{r'}}}{\left|\vec{r_\perp}-\vec{r_\perp'}+\left(2H+z'+z\right)\vec{z_0}\right|}\right\}+\frac{q_{\vec{r}}}{a/2}-\frac{q_{\vec{r}}}{2\left(H+z\right)}\right)+\varphi_0, \qquad (1)$$

where $q_{\vec{r}}$ and $q_{\vec{r'}}$ are charges located at the space-grid nodes with radius vectors $\vec{r}=\{\vec{r_\perp},z\}$ (observation point; the last two terms in the parentheses) and $\vec{r'}=\{\vec{r_\perp'},z'\}$ (source points; the first two terms in the parentheses), respectively, ε_0 is the electric permittivity of vacuum, a is the grid spacing, $H=850$ m is the height of the lower boundary of the computational domain above ground, which corresponds to $z=0$, $\vec{z_0}$ is the upward-directed unit vector of the z-axis, and φ_0 is the background potential associated with the cloud charges (specified via constant

electric field E_0) and charges deposited on the previously-created channel. The summation in formula (1) is performed over all the grid nodes and their images (ground is assumed to be perfectly conducting), excluding the one at which the potential is calculated. In the latter case, the node potential is estimated as its charge divided by one-half of the grid spacing and the corresponding image node potential as its charge divided by $2(H+z)$ (see the last two terms in the parenthesis). The background potential φ_0 at each grid point was specified as

$$\varphi_0(\vec{r}) = \frac{1}{4\pi\varepsilon_0} \sum_{\vec{r'}} \left\{ \frac{q_{\vec{r'}}(\vec{r_\perp})}{\left|\vec{r}-\vec{r'}\right|} - \frac{q_{\vec{r'}}(\vec{r_\perp})}{\left|\vec{r_\perp}-\vec{r_\perp'}+(2H+z'+z)\vec{z_0}\right|} \right\} - E_0 z, \tag{2}$$

where summation is performed over all the nodes with radius vectors $\vec{r'} = \{\vec{r_\perp'}, z'\}$ belonging to the pre-existing leader channel with radius $R=9$ m and containing point charges, magnitudes of which are independent on z and are specified as
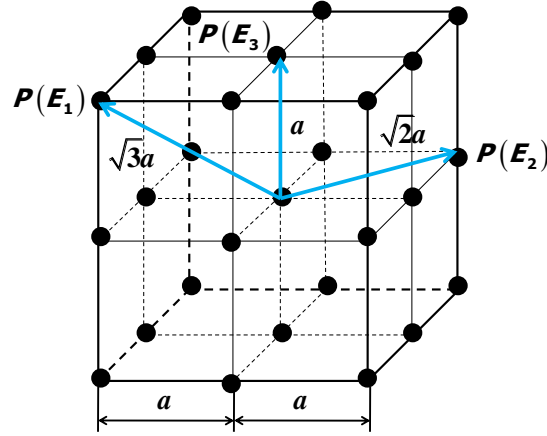
$$q_{\vec{r}}(\vec{r_\perp}) = \begin{cases} q_0, \ \vec{r_\perp} = \vec{r_\perp^0} \\ \dfrac{q_0}{\left|\vec{r_\perp}-\vec{r_\perp^0}\right|}, \ 0 < \left|\vec{r_\perp}-\vec{r_\perp^0}\right| \le R \\ 0, \ \left|\vec{r_\perp}-\vec{r_\perp^0}\right| > R \end{cases}, \tag{3}$$

where $q_0 = 397$ μC is the magnitude of charges at the pre-existing leader channel sheath vertical axis with $\vec{r_\perp} = \vec{r_\perp^0}$. It's assumed that the 300-m-long previously-created channel contains the nodes of Cartesian coordinate system (upward extension of the computational domain), which are enclosed by a cylindrical surface specified by $1150 < z[\text{m}] < 1450$ and $0 \le \left|\vec{r_\perp}-\vec{r_\perp^0}\right| \le R$ (see Fig. 1).

Electric field strength $\vec{E}_{\vec{r},\vec{r'}}$ between two grid nodes with radius vectors $\vec{r}$ and $\vec{r'}$ is calculated as

$$\vec{E}_{\vec{r},\vec{r'}} = -\left(\varphi(\vec{r}) - \varphi(\vec{r'})\right) \cdot \frac{\vec{r}-\vec{r'}}{L \cdot \left|\vec{r}-\vec{r'}\right|}, \tag{4}$$

Where $L = \{(6+12\sqrt{2}+8\sqrt{3})/26\} a \approx 4.25$ m is the average length of 26 possible paths of discharge growth (see Fig. 2), which we used to avoid the dealing with different extension path lengths (ranging from a to $\sqrt{3}a$) in the model.

Figure 2. Possible directions (a total of 26, 3 of which are shown by blue arrows) of discharge extension in the three-dimensional space (grid nodes are represented by black circles). $P(E_1)$, $P(E_2)$, and $P(E_3)$ are the breakdown probabilities, given by Eq. 5, corresponding to the 3 blue arrows.

3) Electric fields required for discharge initiation and propagation

In this work, we will deal with creation of new floating channel segments and extension of existing channels. In either case, the electric breakdown is required and it can occur only between the neighboring nodes of the grid. Any new link has a low initial conductivity ($\sigma_0 = 10^{-5}$ S/m) and is classified as a streamer, although it can be a multiple-streamer formation. A streamer link can either decay or make a transition to a leader link if its conductivity exceeds a threshold value assumed here to be 1 S/m. Leader links that are much less likely to decay contribute to the growth of the discharge tree, while all the decayed links serve to redistribute the space charge. Specific mechanisms of streamer-to leader transition implemented in our model are described in section 3 of the present paper.

A necessary condition for a new floating link creation is that the electric field between two neighboring nodes exceeds the initiation threshold value. If the breakdown has already started, its further development requires electric field exceeding the propagation threshold value, which is considerably lower than the initiation one.

Initiation E_{ith} and propagation E_{pth} threshold fields in numerical models of lightning development depend on grid spacing and, hence, should be viewed as effective [e. g., *Mansell et al.*, 2002; *Iudin et al.*, 2017]. In this study, we assume a factor of 2 different threshold fields for positive (superscript "+") and negative (superscript "-") polarities: $E_{ith}^{+} = 1.34$ MV/m, $E_{ith}^{-} = 2.68$ MV/m, $E_{pth}^{+} = 0.31$ MV/m, and $E_{pth}^{-} = 0.62$ MV/m at an altitude of 1 km, which corresponds to the height of our computational domain center above ground level. Similar streamer propagation fields were obtained experimentally by *Allen and Mikropoulos* [1999] and theoretically estimated by *Gallimberti et al* [2002] for positive polarity, and adopted for both polarities in a number of lightning development models [*Tan et al.*, 2006; *Mansell et al.*, 2010; *Iudin and Davydenko*, 2015; *Iudin et al.*, 2015, 2017]. Note that in this study E_{ith}^{+} and E_{ith}^{-} apply only to the initiation of first streamers from the node representing the space stem and that,

because of $E_{ith}^- > E_{ith}^+$, the first streamer is always positive and, hence, E_{ith}^- is not needed in modeling the initiation of streamers from the space stem. Further, we used reduced initiation threshold fields $E_s^+ = 0.67$ MV/m and $E_s^- = 0.81$ MV/m for subsequent positive and negative streamers (discussed below) initiated from the space stem, respectively.
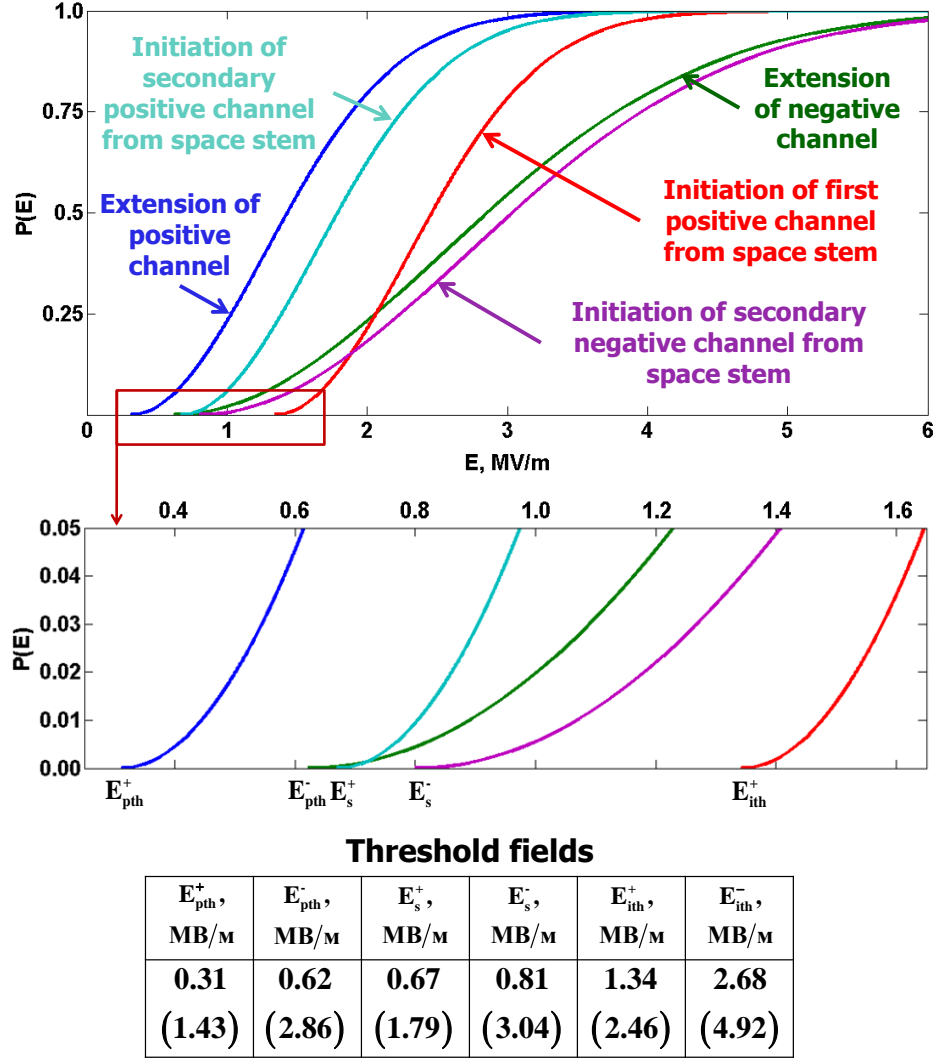
For the case of extension of existing channel, stochastic nature of discharge development is implemented via the distribution function which gives the breakdown probability in a given direction, taking into account both the initiation (E_{ith}) and propagation (E_{pth}) thresholds. The probability of breakdown between a pair of grid nodes with the radius vectors $\vec{r}$ and $\vec{r}'$ is given by:

$$P\left(E_{\vec{r},\vec{r}'}\right) = \begin{cases} 1 - \exp\left[-\left|\dfrac{E_{\vec{r},\vec{r}'} - E_{pth}}{E_{ith}}\right|^m\right], & E_{\vec{r},\vec{r}'} \geq E_{pth} \\ 0, & E_{\vec{r},\vec{r}'} < E_{pth} \end{cases}, \qquad (5)$$

where m is the index determining the steepness of the breakdown probability function (we set $m = 2$ in this study). This probability is zero if the electric field strength E between two adjacent nodes is below the corresponding propagation threshold and increases with increasing E. An overview of the discharge growth probability functions employed in different models is found in work of *Iudin et al.* [2017]. Expression (5) also applies to the case of new floating channel formation, provided that E_{pth} is replaced with E_{ith} (initiation of the first (positive) streamer link from the space stem) or E_s (initiation of subsequent (positive or negative) streamer link from the space stem). As noted above, the initiation of the first negative streamer link from the space stem is not considered in this study as unrealistic. The breakdown probability function (5) is graphically shown in Fig. 3 for the following five cases: initiation of the first positive streamer (E_{Ith}^+) and subsequent positive (E_s^+) and negative (E_s^-) streamers, all from the space stem, and extension of existing positive (E_{pth}^+) and negative (E_{pth}^-) channels. Note that $E_{pth}^+ < E_{pth}^- < E_s^+ < E_s^- < E_{ith}^+$, with

$$\begin{cases} E_{pth}^- = 2 \cdot E_{pth}^+ \\ E_s^- = 1.2 \cdot E_s^+ \end{cases}. \qquad (6)$$

The use of reduced thresholds E_s for subsequent streamer initiation in our model allowed us to reproduce the experimentally observed negative streamer initiation from space stems and, thus, to correctly describe the evolution of space leaders. If we employed only two thresholds, E_{pth} and E_{ith}, there would be a vanishingly small number of negative streamers originating from the space stem. Physically, the reduced thresholds for subsequent streamers, $E_s < E_{ith}$, can be explained by polarization and elongation of the space stem after the first streamer initiation. The elongation of space stem along the local electric field should lead to reduction of effective electric field needed for initiation of subsequent streamer from the space stem. Note that, in contrast with E_{pth}, $E_s^- \neq 2E_s^+$. This was needed to limit the number of positive streamers originating from the space stem. The selected threshold fields allowed the proper reproduction of the observed development of negative stepped leaders.

Figure 3. The breakdown probability functions (top panel) and their enlargements to better show the threshold fields (bottom panel) given by Eq. (5) for the cases of extension of existing positive and negative channels, as well as for 3 other cases corresponding to the initiation of first positive channel (streamer) from the space stem (when E_{pth} in Eq. 5 is replaced with E_{ith}^+) and initiation of second positive and negative channels (when E_{pth} in Eq. 5 is replaced with E_s^+ or E_s^-, respectively). The field thresholds are marked in the bottom panel and their values are given in the table, below the plots, with 50% fields (corresponding to $P(E) = 0.5$) being given in the parentheses. The breakdown probability function for initiation of first negative channel from the space stem is not shown, because the first streamer initiated from the space stem is always positive, but the value of E_{ith}^- is given in the table.

4) General leader development algorithm

The overall leader discharge tree develops as described next, with the simulated leader stepping mechanism being described in section 3. At each time step, any node belonging to the positive or negative part of discharge tree can create a new positive or negative link, respectively,

with any neighboring node of the grid, which doesn't belong to the part of discharge tree of the same polarity, with the probability given by formula (5). The only exception are nodes simulating space stems, which can produce links of both polarities. Creation of such a link (originating from the existing discharge tree) is referred to here as propagation. Further, any free node can give rise to a new floating positive link with a neighboring node. Creation of such a link is called here initiation and the node giving rise to this link is designated a space stem. It is worth noting that the first positive streamer can occur along the path of existing negative streamer from the primary negative leader streamer zone. Note that the algorithm doesn't allow formation of loops in the discharge tree.

The basic element of the discharge tree is the conducting link, which represents a discharge channel (initially a low-conductivity streamer formation which may or may not make transition to a leader channel) between a pair of nodes. Peripheral links of the tree are more likely to remain at the streamer stage and decay. Negative streamers from the primary negative leader streamer zone never make transition to the leader stage and eventually decay.

A newly formed link facilitates charge transfer between the two nodes it connects. When positive charge is transferred to one of those nodes, equal amount of negative charge is placed at the other one and vice versa. The magnitude of charge transferred between two adjacent nodes with radius vectors $\vec{r}$ and $\vec{r}'$ is found as $\delta q_{\vec{r},\vec{r}'} = \alpha E_{\vec{r},\vec{r}'}$, where α is set to $1.26 \cdot 10^{-11}$ (C·m)/V. As an example, for electric field values, under which channel extension probability $P(E)$ is 0.5 (50%) (see Fig. 3), charges separated by a newly-formed streamer link are 18 and 36 µC for positive and negative polarity, respectively.

Parameter α largely determines the amount of shielding of the negative leader channel tip. During the negative corona streamer burst, completing the step formation process (see section 3), negative streamers inject negative space charge in the region in front of the negative leader tip, decreasing the electric field at its vicinity. Larger values of α lead to stronger electric field reduction inside the negative leader streamer zone volume, which opposes the connection of space and primary negative leaders. This results in less negative leader branching and larger both interstep time intervals and space leader lengths. The length of space leaders increases with increasing α, because they have more time to develop before making contact with the primary negative leader channel. Model testing shows that a fivefold increase of α (relative to the selected value) makes negative leader propagation impossible. The use of smaller α reduces negative leader tip shielding and leads to its more intense branching and smaller interstep time intervals and space leader lengths. For example, for a tenfold decrease of α, the negative leader with feeding current of 100 A forms 4 stable branches instead of just 1 for the selected value $\alpha = 1.26 \cdot 10^{-11}$ (C·m)/V (see section 4). The chosen value of α provides satisfactory reproduction of observed negative stepped leader morphology and its electrical and other parameters summarized in Tables 1-4.

Channel conductivity σ in our model is a function of time and is determined by the balance between the production and dissipation of Joule heat in the channel [e.g., *Iudin et al.,* 2017]. As a first approximation, the evolution of channel conductivity can be described by the following equation [*Rompe and Weizel*, 1944; *Dulzon et al.*, 1999; *Iudin et al.*, 2017]:

$$\frac{\partial \sigma}{\partial t} = \left(\eta E^2 - \beta \right) \sigma, \tag{7}$$

where η and β are parameters which represent the rates of channel heating and cooling, respectively. In this study, the following recurrent form of equation (7), written for a pair of nodes with radius vectors $\vec{r}$ and $\vec{r}\,'$, was used:

$$\sigma_{\vec{r},\vec{r}\,'}(\tau + 1) = \left\{ 1 + \left(\eta' E_{\vec{r},\vec{r}\,'}^2 - \beta' \right) \right\} \sigma_{\vec{r},\vec{r}\,'}(\tau), \tag{8}$$

Where $\sigma_{\vec{r},\vec{r}\,'}(\tau)$ and $\sigma_{\vec{r},\vec{r}\,'}(\tau + 1)$ are the conductivity values at the current and the following steps of the computational procedure, respectively, $\eta' = \eta\tau$, $\beta' = \beta\tau$, and $\tau = L/v_{str} = 2.12$ µs is the model time step averaged over all possible discharge tree growth directions (see Fig. 2) and computed for the average extension path length $L = 4.25$ m and assumed streamer propagation speed $v_{str} = 2 \cdot 10^6$ m/s (the minimum observed values given by *Bazelyan and Raizer* [2000, p. 39] for positive streamers in sparks are $(1.5\text{-}2) \cdot 10^5$ m/s). In this study, parameter η', responsible for channel conductivity increase, is assumed to be constant and set to $6 \cdot 10^{-13}$ m^2/V^2, while parameter β' determining the rate of conductivity decrease at step $(\tau + 1)$ is a function of channel conductivity at step τ:

$$\beta_{\vec{r},\vec{r}\,'}' \left(\sigma_{\vec{r},\vec{r}\,'}(\tau) \right) = 10^{-5} \left(1 + \exp\left(\frac{\sigma_{\vec{r},\vec{r}\,'}(\tau)}{\bar{\sigma}} \right) \right), \tag{9}$$

where $\bar{\sigma} = 10^4$ S/m is the expected conductivity of hot leader channel core. The initial value of newly-formed discharge channel conductivity σ_0 is set to 10^{-5} S/m, which is close to the expected conductivity of streamer formations [e.g. *Maslowski and Rakov*, 2006].

Equation (9) describes exponential channel cooling rate increase with increasing channel conductivity. Although the actual form of dependence (9) is unknown, it is reasonable to assume that there is faster cooling for higher-conductivity (higher-temperature channels). This is the case because the radiation energy losses which, in a blackbody approximation and according to the Stefan-Boltzmann law, are proportional to the fourth power of the plasma temperature. Further, the heat flux from the channel surface increases with increasing channel temperature because the temperature gradient between the channel and the environment is larger for a higher-temperature channel.

Note that the link (channel) in our model is a virtual object: one can view it as a rectangular slab or as a thin cylinder, and the only parameter that depends on the cross-sectional area is conductivity. In this study, we assumed that, as discussed below, the channel radii of links belonging to the main negative leader structure with feeding currents I_b of 104, 214, and 347 A are 0.58, 0.83, and 1.05 mm, respectively, while the radii of channels belonging to space streamers / leaders are 0.20 mm, regardless of I_b.

The electric field along a link is found as the potential difference between the nodes at its ends divided by the length of the link. This field gradually relaxes from the pre-breakdown value to the hot-channel value (if the streamer-to-leader transition takes place) of 10^4 V/m [*Mansell et al.*, 2010] under the action of potential equalization (field relaxation) currents flowing through all

the discharge tree channels [*Iudin et al.*, 2017]. For each link, joining nodes with radius vectors $\vec{r}$ and $\vec{r}'$, this current is found from Ohm's law as

$$I_{\vec{r},\vec{r}'} = \sigma_{\vec{r},\vec{r}'} \pi r^2 E_{\vec{r},\vec{r}'}. \tag{10}$$

The field-relaxation currents given by (10) lead to polarization of the entire conductive discharge tree in the overall electric field in the computational domain and to charge accumulation at the channel branch tips. This means that the electric field decreases in the interior of the discharge tree with its simultaneous intensification at the discharge tree periphery [*Iudin et al.,* 2017].

We now discuss the method of feeding of (supplying negative charge to) the growing discharge tree in our model. Lightning leaders prior to their connection to the ground, have both positive and negative parts (see, for example, *van der Velde and Montanyà* [2013]; *Kostinskiy et al.* [2015b]). The charge redistribution between those two parts occurs in such a way that the positive part acts as a source of negative charge for the negative one and vice versa. Since the entire discharge tree is to be electrically neutral, the negative charge transferred to the negative part by currents, given by (10), from the positive part must be equal in absolute value to the positive charge transferred to the positive part. In our model, the positive part is not simulated (see Fig. 1), and charge is constantly supplied to the initial (upper) node of the negative part of the simulated discharge tree via the feeding current I_b. This current is assumed to rapidly increase with time from zero to its maximum (steady-state) value I_0 according to the following equation:

$$I_b(t) = I_0 \cdot \mathrm{cth}\left(t/\bar{\tau}\right), \tag{11}$$

where $\bar{\tau} = 15 \cdot \tau \approx 32$ µs. In this study, calculations were performed for 3 values of I_0, 100, 210, and 350 A, which are within the range of expected average lightning leader currents [*Rakov and Uman,* 2006, ch. 1.4, p. 7]. In the following, the 3 values of I_0 given above are accompanied by label I_b. Charge redistribution associated with currents given by (10) in all discharge tree links is normalized so that the current injected into the initial node of the modeled negative leader from all discharge-tree channels is equal to $I_b(t)$. To ensure the stability of numerical scheme, this charge renormalization procedure takes place every $\tau_s = 1.42$ ns, where subscript "s" stands for small and is used to differentiate τ_s from the model time step $\tau = 2.12$ µs, which is 1500 times larger than τ_s. Thus, positive charge entering the initial node from the negative-leader channel structure below it is compensated by the equal amount of negative charge supplied by feeding current $I_b(t)$. One can view this charge normalization as adjustment of the radii of channels belonging to the negative-leader tree, which vary in time to maintain the required potential equalization currents given by (10). At the same time, there is no recalculation of charge variation in the channels of space streamers / leaders. As a result, their channel radii are constant and are set to $2 \cdot 10^{-4}$ m. Note that such an algorithm allowed us to avoid (compensate for the non-physical) charge accumulation at the discharge-tree initial node that is associated with the deposition of negative charge onto the extending negative-leader channel.

In the present study, the positive part of the discharge tree is replaced with an artificial feeder connected to the initial node of the negative part at the upper boundary of the computational domain. Because of that, the longitudinal electric field and, consequently, the conductivity of the initial channel segment in the computational domain requires special treatment. We assume that the initial channel segment is characterized by constant magnitudes of longitudinal electric field $E_b = 10^4$ V/m (see *Bazelyan and Raizer* [2000, p. 204]) and conductivity $\sigma_b = 10^4$ S/m (see *Rakov and Uman* [2003, p. 164]). Those values are typical for an established leader channel, which is similar to an electric arc. Calculations based on Ohm's law show that a leader channel with conductivity σ_b and longitudinal electric field E_b must have radii of the current-currying core of 0.58, 0.83, and 1.05 mm for the feeding currents I_b of 100, 210, and 350 A, respectively.

As noted above, it is assumed in this study that any newly-added channel segment is initially a low-conductivity ($\sigma = 10^{-5}$ S/m) streamer formation, which can be transformed, via Joule heating, into a well-conducting leader channel. We use the channel conductivity as the criterion of streamer-to-leader transition with the threshold value being $\sigma_{th} = 1$ S/m. This value is typical for both the streamer head [*Raizer*, 2009] and for the newly-formed positive laboratory leader channel carrying a current of 1 A [*Raizer*, 2009, p. 602]. We additionally considered values of σ_{th} ranging from 0.1 to 10 S/m and found no significant differences in model-predicted negative leader parameters, except for interstep intervals, which approximately double for $\sigma_{th} = 10$ S/m, thus, decreasing the negative leader speed. We assumed in this study that all new channel segments originating from the negative leader tip are streamers and caped their conductivity at 1 S/m, so that they remained streamers indefinitely, regardless of current they carry. This was needed to emphasize the stepped nature of the modeled negative leader development. If we did not cap their conductivity at 1 S/m, some of them would make transition to the leader stage, thus contributing to the negative leader continuous propagation, which, in principle, can occur, but we decided to suppress it in the present study. On the other hand, streamers of either polarity developing from space stems were allowed to evolve into leaders, which facilitate the step-wise extension of negative leader channel. Possible propagation of space stem between steps (see, for example, [*Gorin and Shkilev,* 1976]) was neglected.

Most space streamers never become space leaders and, hence, do not produce steps. If the first positive streamer initiated from the space stem comes in contact with the negative leader channel, it is removed with the separated space charges being conserved. We refer to such space stems creating "premature" streamer connection to the main channel as "failed space stems". Further, some discharge tree branches (even if they are at the leader stage) may stop growing, lose connection with the main discharge tree, and decay. In this study, the condition for the peripheral branch decay was considered to be met if during one time step no new links were initiated from its tip (one exception from this rule is described in the next paragraph). The charge previously transported to the node corresponding to the decayed branch tip (or to both tips if the decaying structure is a single floating link) remains "frozen" at that node (or nodes), because of the low conductivity of the medium and the relatively small time (compared to the charge relaxation time) needed for the discharge development (see Table 2). The process of "freezing"

the space charge near the main leader channel contributes to the formation of the leader corona sheath (see, for example, *Bazelyan and Raizer* [2000, Fig. 2.2]). As noted in Section 1, another contributor to the corona sheath is the radial corona current (see, e. g., *Maslowski and Rakov* [2006]) from the channel core, which is not considered in our model.

In our model, the life time of a channel segment is determined by the probability of its decay, whose dependence on conductivity σ is assumed to be as follows:

$$P_d(\sigma) = 1 - \mathrm{cth}(\sigma/\sigma_m), \tag{12}$$

where $\sigma_m = 10^4$ S/m is the conductivity above which a channel segment is assumed to become essentially "immortal", even if no new links originated from it. Also, the initial link at the top of the downward extending discharge tree is set to be "immortal".

Note that in our model channel development and decay may be occurring simultaneously in different parts of the discharge tree, and that the number of links originating from the same parent node is limited to 26 (see Fig. 2).

Simulation stops when a branch of the primary negative leader touches one of the boundaries of the cubical computational domain.

SIMULATION OF LEADER STEPPING MECHANISM

Our model allowed us to simulate, for the first time, the negative-stepped-leader propagation mechanism described in section 2.3. This would not be possible without considering the polarity asymmetry (see Appendix A). The sequence of processes involved in the formation of negative leader step is schematically shown in Figure 4. The leader stepping algorithm implemented in the model is as follows:

(1) The negative corona streamer burst originating from the just-formed negative leader tip and completing the previous step formation process rapidly injects a large amount of negative charge into the space ahead of the leader tip. This streamer burst is seen at stage A in Fig. 4.

(2) The injected space charge creates highly non-uniform electric field in front of the negative leader tip. As a result, highly-localized plasma seeds (space stems) are formed inside or near the negative space charge region (corona streamer burst). In Fig. 4, three competing space stems are shown below the corona streamer burst at stage B.

(3) Space stems launch positive streamers toward the primary negative leader channel, building up the potential for launching negative streamers in the opposite direction. As a result, bidirectional space streamers originating from the space stem are formed.

(4) As the space streamers are heated by polarization current and their conductivity increases, they may become space leaders. Since the positive part is formed earlier, it can reach the leader stage, while the negative part is still at the streamer stage or even absent. Both scenarios are seen at stage C in Fig. 4. In the latter case, the charge is conserved by placing negative charge on the stem as the positive part extends toward the primary channel.

For simplicity, the following description refers to a single space leader.

(5) The positive end of space streamer / leader moves toward the primary (negative) leader channel until the former comes within a single extension increment of the primary leader tip (see stage C in Fig. 4).

(6) If the link separated from the primary leader tip by a single extension increment is sufficiently conducting (at the leader stage), a new streamer link connects the positive end of the space leader to the primary (negative) leader channel. This link is labeled "Streamer connection between space and primary leader channels" in Fig. 4 (see stage D).

(7) Connection of the floating space leader channel to the primary leader channel causes rapid rearrangement of charge distribution in the entire discharge tree, from the negative end of the space leader (or from the position of corresponding space stem, if the negative part of the space leader failed to form by this time) to the primary negative leader initial node. The resultant current heats all the channel segments that it traverses, so that their conductivity increases. The negative leader tip is transferred to the former space-leader negative end (or to the position of the space stem), causing a negative corona streamer burst (see stage E in Fig. 4). The negative streamer channels (if any) of the space leader become part of the corona streamer burst.
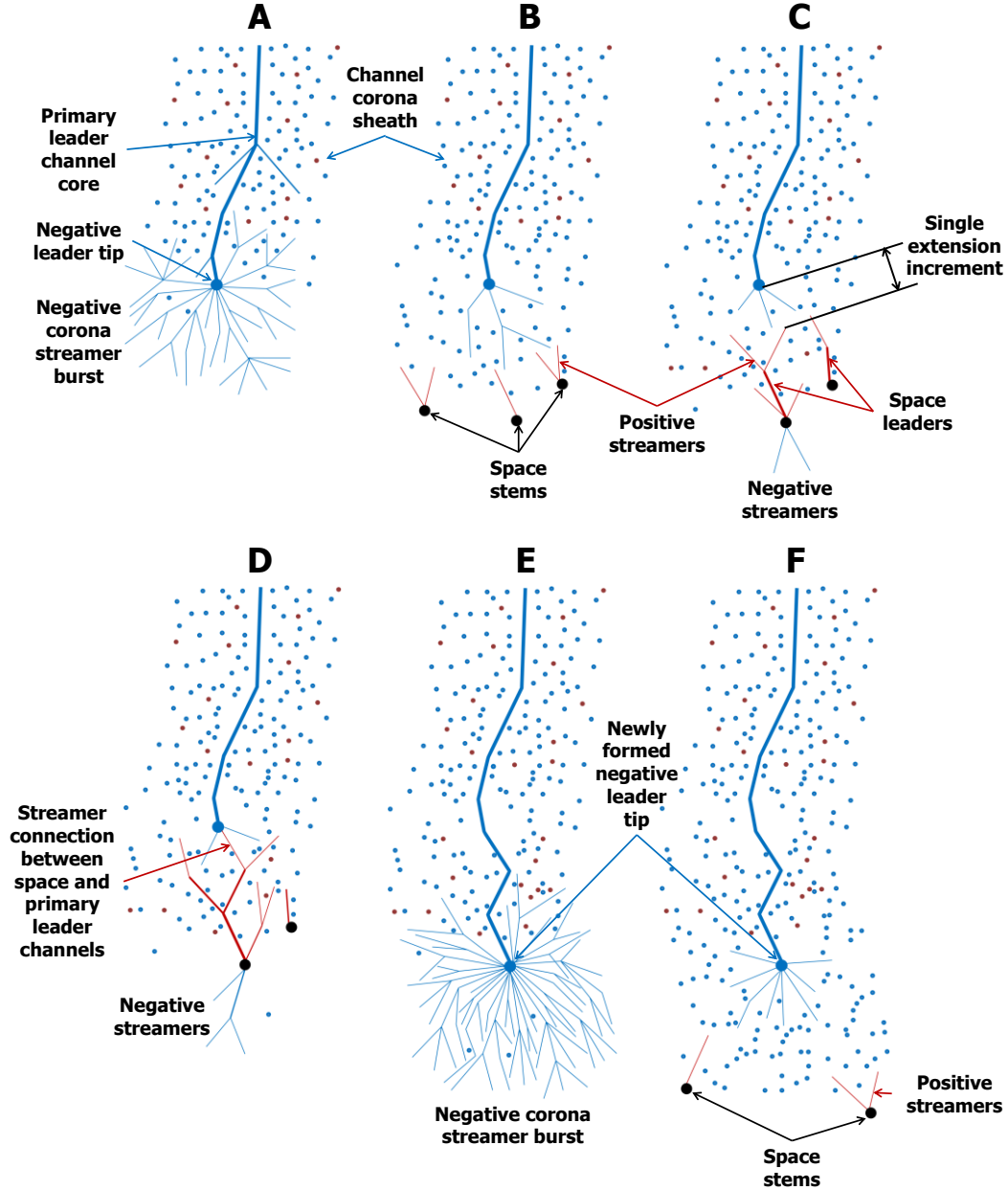
(8) The process repeats itself (see stage F in Fig. 4, which is similar to stage B).

It's important to stress that in this work the space stem is just a node which doesn't belong to the primary negative leader channel system, which acts as the origin of positive and negative space streamers.

If at a given time the electric field between a node which does not belong to the existing discharge structure, which we refer to as a potential space stem, and another (not necessarily free) node nearby exceeds the initiation threshold E_{ith}, then with the probability given by formula (5) a streamer link bridges these two nodes. Note that because of the polarity asymmetry (see Appendix A) the unrealistic scenario, when a space stem produces negative streamers (growing against the electric field direction) before positive ones (growing along the electric field direction) does not occur in our model. The space stem can subsequently become the origin of other positive and negative streamers if the electric field between this and neighboring nodes exceeds the subsequent initiation threshold fields $E_s^+ = 0.67$ MV/m and $E_s^- = 0.81$ MV/m, respectively, which, as noted above, are set to be lower than the corresponding initiation threshold fields, but higher than the propagation ones. The ratio of positive to negative thresholds for subsequent initiation (0.84) is set to be larger than for first initiation (0.5) in order to promote initiation of subsequent negative streamers from the space stem. Note that we allow the positive streamer / leader links originating from the space stem to overlap the existing channels of the negative-leader streamer zone, but not the existing positive links. In the case of link overlapping, both links independently contribute to the current given by (10).

Positive streamers of the space leader often come in contact with the primary (negative) leader channel, but this doesn't always result in a new step. The necessary condition for step formation used in this study is a sufficiently high conductivity, equal to or higher than $\sigma_{th} = 1$ S/m, on both sides of the final streamer link (streamer connection) bridging the space and primary leader channels (see stage D in Fig. 4). In other words, the links on both sides of the final streamer link must each be at the leader stage of development. If this criterion isn't met, the positive streamer link which came in contact with the negative leader channel dies out leaving

behind the charges it caused to separate (to be transferred). Once the two leaders (whose conductivity exceeds 1 S/m) are connected via a streamer link with the initial conductivity $\sigma_0 = 10^{-5}$ S/m, it is assumed that the step-formation process cannot be reversed. In the following, we describe how streamer links evolve into leader links in our model.

Figure 4. Schematic representation of the step formation process. The complete cycle (A-E) usually takes a few tens of microseconds. Dark-red and blue colors correspond to positive and negative polarities, respectively, and black dots represent space stems. Thicker lines correspond to higher conductivities. Positive and negative space charges in the leader channel corona sheath are denoted by dark-red and blue dots, respectively.

At the end of each time step, all existing channel segments are divided into two categories. Included in the first category are only links between the initial (upper) node of the primary negative leader and the nodes corresponding to the negative tips of space leaders (or the nodes corresponding to space stems, if the negative parts of the space leaders failed to form by that time), which were involved in formation of new steps that merged with the primary leader channel during this time step. Thus, the channel segments of the first type are those involved in the stepwise extension of the negative leader (potentially all the way up to the initial node) at this time step. All other channel segments are included in the second category. For each channel segment (regardless of its category) the conductivity and current are recalculated using formulas (8) and (10), respectively. As noted above, the charge variation, associated with current (10), occurs on the time interval $\tau_s = 1.42$ ns, which is much smaller than the model time step $\tau = 1500\tau_s = 2.12$ μs. The conductivity of channels in the first category is recalculated 50 times, at every thirtieth small time step τ_s, while the conductivity of channels of the second type is recalculated only once, in the middle of the charge variation process. Any changes in the charge configuration at the end of each small time step ($\tau_s = 1.4$ ns) are accompanied by the electric potential recalculation using formula (1). Variation of charges located at nodes that belong to the primary leader channel are normalized so that the charge flowing from all these nodes into the feeding (initial) node is consistent with the magnitude of the feeding current (11).

Any unconnected branches of the positive part of space leader (regardless of σ) are "switched off" at the time of the space leader making connection to the primary leader via the final streamer link. The positive charges residing at the far end of those unconnected branches contribute to the space charge region surrounding the leader channel. Note that the net charge near the leader channel is negative and that in our model this charge is almost exclusively associated with corona streamer bursts completing the step-formation process (further discussed in Section 5 and Appendix A).
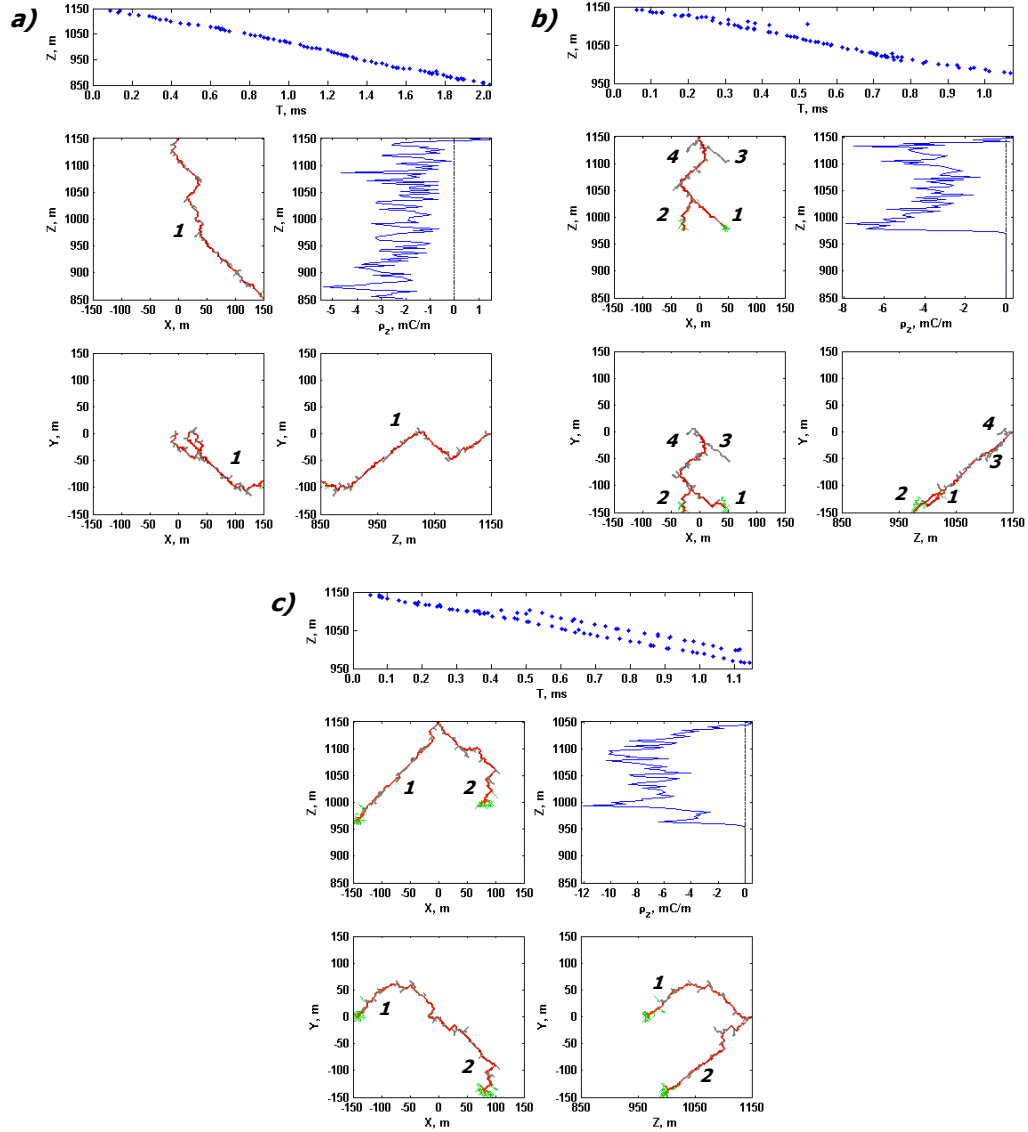
RESULTS

Figure 5 presents 2D projections onto the x-y, x-z, and y-z planes of 3 modeled negative stepped leaders within roughly 1 km above ground with feeding currents of 100, 210, and 350 A. Also shown for each of the 3 events is the leader tip height above ground versus time and the line charge density in the leader channel corona sheath ρ_z versus height. Figure 6 shows the three-dimensional negative leader channels, whose 2D projections are seen by Figure 5, as well as the lower part of the leader with 210-A feeding current to better resolve the fine structure of streamer zones at leader branch tips.
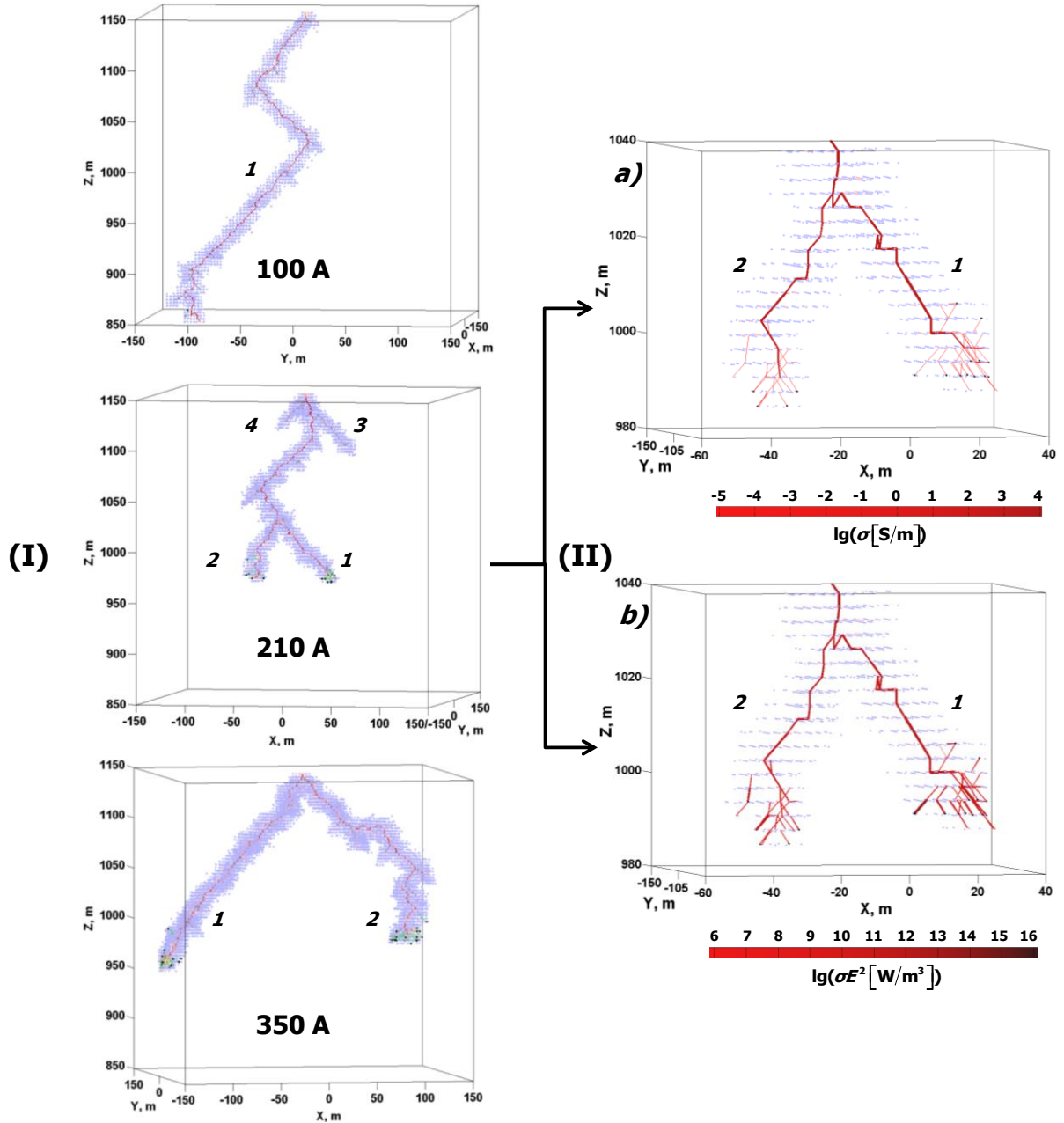
The morphology of simulated negative leader channels shown in Figures 5 and 6 is similar to that seen in high-speed video images of negative lightning [*Hill et al.*, 2011; *Petersen and Beasley*, 2013; *Tran et al.*, 2013; *Lu et al.*, 2016; *Qi et al.*, 2016; *Jiang et al.*, 2017]. Note in Fig. 6(II) the multiple space streamers / leaders (mostly space streamers) simultaneously existing in the vicinity of each negative leader tip. Branching of the negative leader channel is caused by the random nature of space leader attachment to the primary channel, which is in agreement with recent optical observations reported by *Tran et al.* [2014] and *Jiang et al.* [2017]. Space leaders which connect to the negative leader tip lengthen the existing channels, while those connecting to

the lateral surface of existing channels, create side branches (one of which can become the main channel). As seen in Figures 5 and 6, some negative leader channels exhibit substantial horizontal extent and even upward progression (for a short distance), which is consistent with observations by *Wu et al.* [2015].

Figure 5. 2D projections onto the x-y, x-z, and y-z planes of 3 modeled negative stepped leaders with feeding currents of (a) 100, (b) 210, and (c) 350 A at the end of the simulation (2.03, 1.07, and 1.15 ms, respectively) shown along with the negative leader tip height versus time and the charge density in the leader channel corona sheath ρ_z at the end of the simulation versus height. Peripheral branches which died out during the discharge tree development process and positive space streamer channels are shown in grey and green, respectively. The corresponding 3D plots, additionally showing space stems and space charges forming the channel corona sheath are presented in Fig. 6. Individual branches here and in Fig. 6 are numbered, with this numbering being the same as in Tables 2-4.

Figure 6. (I) 3D plots of 3 modeled negative stepped leaders with feeding currents of 100, 210, and 350 A at the end of the simulation (2.03, 1.07, and 1.15 ms, respectively). Peripheral branches which died out during the discharge tree development process and positive space streamer channels are shown in grey and green, respectively. Branch numbering is the same as in Figure 5 and in Tables 2-4. Black dots denote space stems and blue and pink dots negative and positive space charges forming the leader channel corona sheath, respectively. (II) The lower part of the leader with the feeding current of 210 A at 958 µs showing the fine structure of streamer zones at leader tips. In (a) the color intensity represents power density dissipated in the channel and in (b) it represents electric conductivity of the channel.

The number of model-predicted streamer branches is larger than seen in optical records. This can be explained by insufficient luminosity of most of the streamer channels [*Rakov and Uman*, 2003, p. 135-136; *Hill et al.*, 2011; *Petersen and Beasley*, 2013; *Wu et al.*, 2015; *Qi et al.*, 2016].

Quantitative characteristics of simulated leaders (see Tables 2-5) are also in good agreement with optical observations (see Table 1). The large ranges of variation of the parameters presented in Table 1 can be attributed to the improvement of optical instrumentation and to the dependence of negative leader stepping parameters on height. It's noted by *Rakov and Uman* [2003, p. 122] and *Wu et al.* [2015] that both interstep interval and step length decrease by an order of magnitude as the leader approaches the ground.

Table 1. Characteristics of natural negative lightning stepped leaders observed using photoelectric systems and framing cameras.

Study	Interstep interval, μs	2D step length, m	2D[a] leader speed, 10^5 m/s
Chen et al.[b] [1999] (Australia)	5.0-50.0	7.9-20	4.9-11.0
Chen et a.l[b] [1999] (China)	18.0-21.0	8.5	4.9-5.8
Lu et al. [2008]	0.2-15.7	-	15.0
Hill et al. [2011]	12.2-40	4.8-7.1	2.7-6.2
Petersen and Beasley [2013]	-	-	5.6
Tran et al. [2014]	-	14, 15	6.5-9
Qi et al. [2016]	13.9-23.9	-	4.1-14.6
Jiang et al. [2017]	6.9[c]	1.3-8.6	-

[a]Except for *Petersen and Beasley* [2013], who measured 1D leader speed.
[b]Studies based on the use of ALPS photoelectric system, as opposed to framing cameras used in all other studies summarized in this table.
[c]Found as the observation period of 667 μs divided by the total number (96) of individual step-wise channel extensions.

The extension speed of simulated negative leaders is of the order of 10^5 m/s (see Table 2). Interstep intervals (see Table 3) vary in the range of 0.53-140 μs with a mean of 30.5 μs. *Hill et al.* [2011] reported the average interstep interval of about 20 μs from high-speed video recordings of natural lightning with interframe intervals of 3.33 μs. The mean step length (see Table 3) is of the order of 10 m. This is smaller than the typical step length of 50 m or so reported from streak-camera observations, but exceeds the more recent values, 1-9 m (see Table 1), obtained using framing cameras. Possible reasons for the disparity in optically measured step lengths found in the literature were discussed by *Hill et al.* [2011]. Also, optically measured step lengths are usually two-dimensional and, hence, may be underestimated. The line charge density of the simulated negative leader branches is about 500 μC/m (see Tables 2 and 4). This is equal to 500 μC/m used in the simulations by *Riousset et al.* [2007], but less than 700-1000 μC/m given by *Rakov and Uman* [2003, pp. 123, 125]). The aggregated line charge density along the vertical axis

of simulated leader is of the order of 1000 µC/m. For comparison, the charge per unit length for the 300-m long pre-existing channel section (see Fig. 1) was set to 800 µC/m.

Table 2. Characteristics of branches of the negative stepped leaders presented in Figs. 5 and 6(I).

Branch number	3D length, m	Start time, µs	End time[d], µs	Life time, µs	3D extension speed[a], 10^5 m/s	Line charge density, µC/m	
						3D[b]	1D[c]
100-A feeding current							
1	540	0	2031	2031	2.66	387	696
210-A feeding current							
1	340	0	1071	1071	3.18	413	1291
2	85	707	1071	364	2.34		
3	71	202	612	410	1.73		
4	48	76	334	258	1.86		
350-A feeding current							
1	345	0	1145	1145	3.01	587	2096
2	319	76	1145	1069	2.98		
Mean for all branches	250	-	-	-	2.54	462	1361

[a]Leader speed for each individual branch (including only sections with conductivity exceeding 1 S/m) was calculated as its length divided by its life time.

[b]Leader charge per unit length is calculated as the absolute value of the ratio of the entire charge transferred into the simulation domain by the negative stepped leader to the total length of its branches (those, which are shown in the table) at the end of the simulation.

[c]The total charge transferred into the simulation domain per unit length along z-axis calculated under the assumption that the leader has a single vertical channel, the length of which is the difference between the heights of the simulation domain top (1150 m) and the lowermost primary leader tip at the end of simulation.

[d]The branch end time is determined by the end of simulation, which stops when one of the branches touches one of the boundaries of the cubical simulation domain.

Electrical characteristics of simulated negative leader steps are summarized in Table 4 and temporal evolution of some parameters associated with these steps are presented in Figures 7 and 8.

Fig. 7 shows a typical example of temporal evolution of conductivity, absolute value of longitudinal electric field strength, current, and power density (I) in the channel section that linked the space leader to the primary leader (that is, the final bridging link) and (II) in the positive part of space leader for the discharge with feeding current of 210 A.

Table 3. Characteristics of stepping of the negative stepped leaders presented in Figs. 5 and 6(I).

Branch number	Number of steps		3D interstep interval, µs			3D step length, m		
	Total	Time-resolved	Min	Max	Mean	Min	Max	Mean
100-A feeding current								
1	88	74	0.7	74.4	22.3	5.2	15.6	9.0
210-A feeding current								
1	55	45	0.7	51.0	18.4	6.0	12.4	9.0
2	13	11	0.7	65.9	30.3	7.2	10.4	8.7
3	7	5	2.1	140.2	53.5	7.2	10.4	9.0
4	5	5	14.9	61.6	43.0	8.5	10.4	9.6
350-A feeding current								
1	56	39	0.5	51.0	19.9	7.2	15.6	10.0
2	39	29	0.7	65.9	25.9	7.2	18.9	10.5
Mean for all branches	38	30	2.9	72.9	30.5	6.9	13.4	9.4

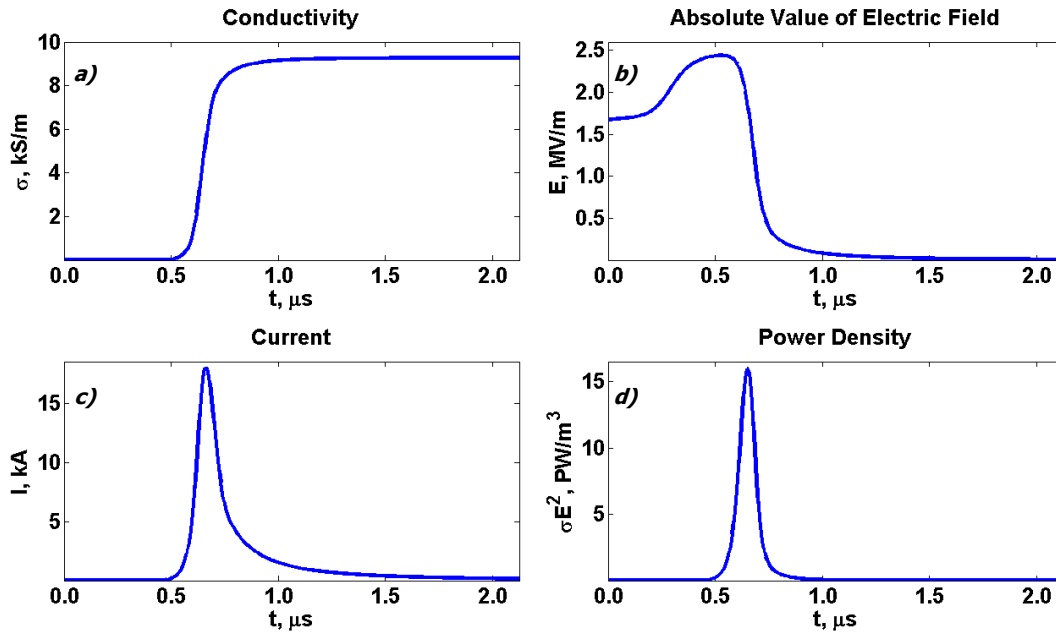**Table 4.** Electrical characteristics of the negative leaders shown in Figs. 5 and 6(I).

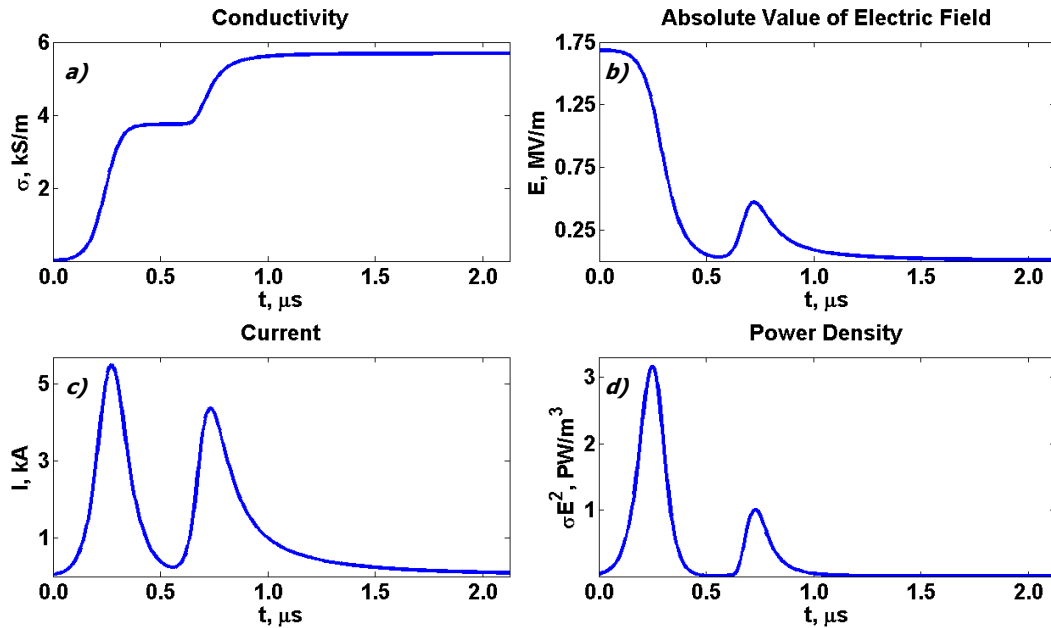| Branch number	Final channel conductivity[a], kS/m			Current peak value[a], kA			Charge transferred to the newly formed leader tip, mC			The line charge density[b], µC/m
	Min	Max	Mean	Min	Max	Mean	Min	Max	Mean	
100-A feeding current										
1	0.02	20.00	14.14	0.01	22.57	10.08	0.05	2.53	1.71	387
210-A feeding current										
1	0.65	9.88	6.65	0.88	20.65	9.16	0.19	5.11	1.80	447
2	1.70	9.12	6.70	1.22	15.28	9.15	1.40	2.17	1.78	449
3	0.05	8.09	6.18	0.08	13.80	8.90	0.04	2.08	1.56	410
4	4.44	6.17	5.21	4.24	8.76	5.99	1.18	1.71	1.39	579
350-A feeding current										
1	0.23	8.28	4.59	0.34	20.20	9.52	0.68	2.54	1.85	639
2	0.03	8.54	5.31	0.06	22.60	11.84	0.80	2.65	2.00	562
Mean for all branches	1.02	10.01	6.97	0.98	17.69	9.23	0.62	2.68	1.73	496

[a]The magnitudes of final channel conductivity and current peak are given for the final streamer link bridging the space-leader and primary-leader channels.
[b]The line charge density of individual branches was calculated without double-counting the nodes found in overlapping channel sheaths of two branches.

(I) Final bridging link

(II) Positive part of space leader

Figure 7. Typical temporal evolution of (a) conductivity, (b) absolute value of longitudinal electric field strength, (c) current, and (d) power density in (I) the final link that bridged the space-leader and primary-leader channels and (II) the positive part of space leader link that originated from space stem during the step-formation process. The feeding current was 210 A. The full time scale corresponds to one model time step (2.12 μs).

The step-formation process leads to a sharp increase of conductivity in the final bridging link, accompanied by longitudinal electric field reduction and sharp current and power density pulses, as expected for the streamer-to-leader transition process. The time interval during which the significant changes in all the presented parameters occur is about 0.3-0.4 µs. The gradual increase of electric field prior to its more rapid decrease can be explained by charge accumulation at the ends of the poorly-conducting streamer channel section which linked the space leader with the primary one. Once the conductivity of that link becomes sufficiently high, its electric field rapidly falls. Note that the step current pulse peak, step current pulse duration (at half-peak level), and the charge transfer expected for negative lightning leaders are 2-8 kA, 0.4-0.5 µs, and 1-4 mC, respectively (see *Rakov and Uman* [2003, p. 132, 134]). The conductivity of lightning leader channel core, according to *Rakov and Uman* [2003, p. 164], is similar to the typical arc conductivity of 10^4 S/m (10 kS/m).

In contrast with the final bridging link, for the positive part of space leader (whose far end for the considered step became the newly-formed negative leader tip) the temporal evolution of each of the examined quantities exhibits two stages. The first one (from 0 to 0.5 µs in Fig. 7(II)) corresponds to the time interval, during which the final bridging link connecting the space leader to the existing leader channel has insignificant conductivity and cannot provide potential equalization between the space and primary leaders. At this stage, the space leader channel continues to polarize as if it were unconnected with the primary one. The first current pulse with the peak of about 5 kA reduces the longitudinal electric field strength and increases the channel conductivity from ~ 1 MV/m to about 30 kV/m and from 1-10 S/m to 4 kS/m, respectively, thus transforming the space leader to an arc-like formation. As the final bridging link conductivity makes a sharp jump (at about 0.5 µs; see Fig7(I)), the second stage in Fig. 7(II) begins, at which the space leader actually becomes part of the primary leader channel. The electric field increase after 0.5 µs in Fig. 7b(II) is caused by charge redistribution between the two highly polarized leader sections, which injects additional negative charge into the newly-formed negative leader tip and transfers positive charge, which was accumulated at the upper end of the space leader upward, potentially all the way up to the initial node. This process is accompanied by potential equalization current pulse, during which the bridging link finally turns into a full-fledged part of the primary negative leader channel (see Fig.7(I)). Note that the two-stage time evolution of quantities shown in Fig. 7(II) is typical for most of the space leader channels involved in the step formation process, although the time interval between the two stages and relative magnitudes of the quantities at the two stages may vary.

Similar two-stage development may take place in the lightning attachment process, which also includes the establishment of streamer connection (common streamer zone) between upward and downward leaders of opposite polarities. It is likely that any connection in lightning and sparks should have two stages: streamer connection and hot-channel connection, each one being associated with an abrupt current rise [*Tran and Rakov*, 2017]. In rocket-triggered lightning streamer connection is associated with a current pulse (current increase from some amperes to some hundreds of amperes; *Hill et al.*, 2016), with hot leader channel connection occurring a couple of microseconds later and being associated with current rise to many kiloamperes.

Sometimes between those two connections there are additional (attempted hot-channel) connections (see *Tran and Rakov* [2017] and references therein). Two current and light pulses have been documented during the attachment process in long negative sparks [*Kostinskiy et al.*, 2016, Figs. 2 and 4].

Fig. 8 shows the current and power density waves in different sections of the channel associated with a single step presented in Fig. 7. 3D distances between the center of each channel section and the newly-formed leader tip are, from bottom to top, 8, 18, 30, 70, 132, and 217 m. As one can see, a new negative leader step produces a sharp pulse (with 18-kA current peak), whose much reduced effect is felt hundreds of meters up along the channel. This behavior is qualitatively consistent with the propagation of step-luminosity pulses from the leader tip up along the channel reported by *Wang et al.* [1999] and *Chen et al.* [1999].

Table 5 presents information about the fine structure and dynamics of space stems, space streamers / leaders, and negative corona streamer bursts. It includes space-leader lengths and occurrence rates of failed and successful space stems, and rates of space streamer / leader death, space leader making connection to the primary leader channel, and occurrence of negative streamers composing the negative corona streamer burst. All the rates are given for the 3 leaders presented in Figs. 5 and 6(I) and are averaged over the entire simulation time. Note that our space-leader lengths are in good agreement with those measured by *Gamerota et al.* [2014], who analyzed high-speed video recordings of dart-stepped leaders in triggered lightning. As one can see in Table 5, a very small fraction (less than 7%) of space stems produce viable space leaders that make connection to the primary leader. The overwhelming majority of space stems produce only positive streamers that touch the primary leader channel and die, leaving behind a pair of space charges contributing to the corona sheath. It is also clear that the dominant charge in the corona sheath is negative and that it is supplied by negative corona streamer bursts.
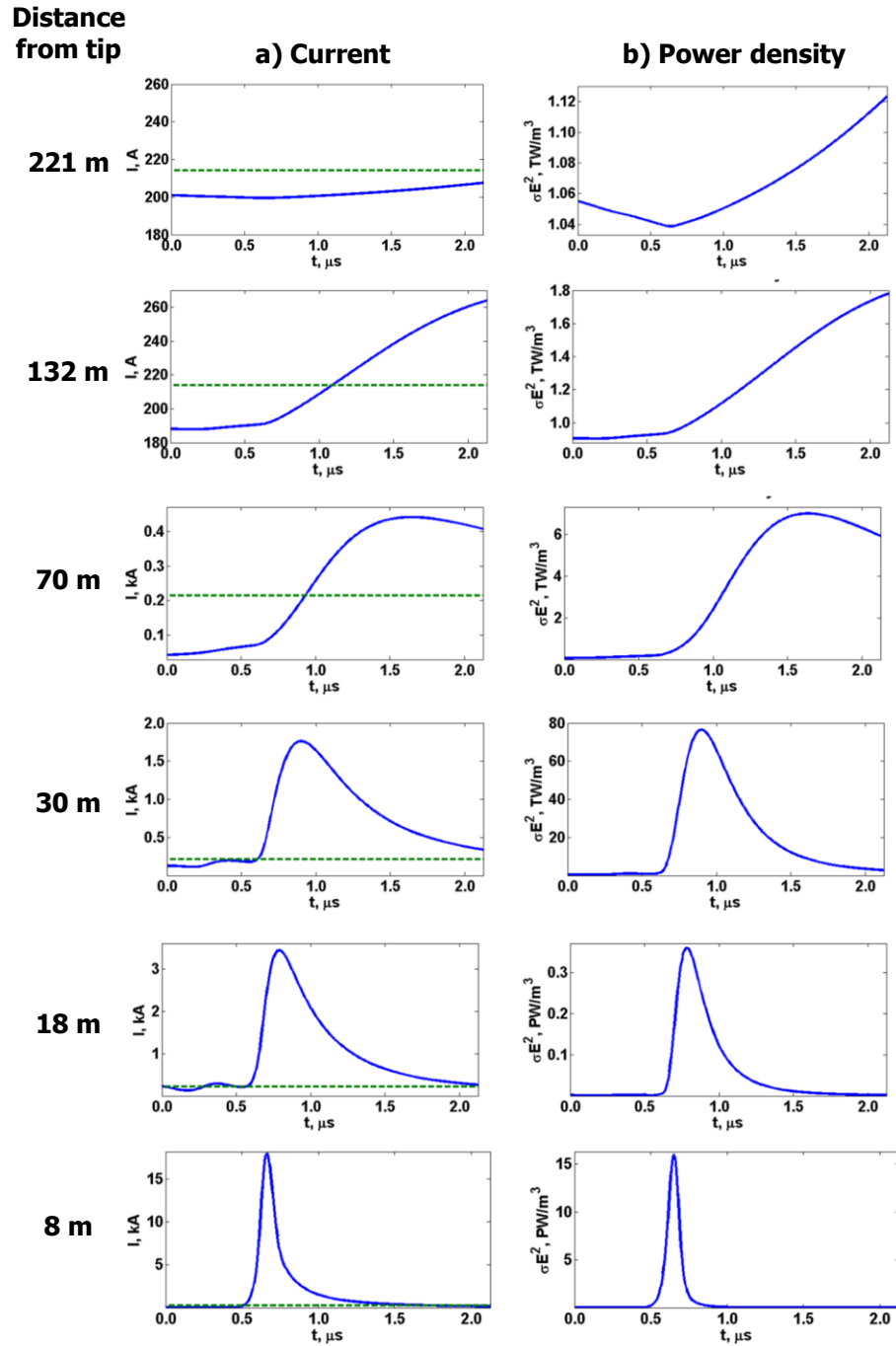
Table 5. Characteristics of space streamers / leaders and negative corona streamer bursts in 3 leaders presented in Figs. 5 and 6(I).

Feeding current, A	Space-leader 3D length, m			Rate of failed space-stem occurrence, MHz	Rate of successful space-stem occurrence, MHz	Rate of space-streamer / leader death, MHz	Rate of space leader connection to the primary channel, kHz	Rate of occurrence of negative streamers in corona streamer burst[b], MHz
	Min[a]	Max	Mean					
100	3.0	5.2	4.7	1.45	0.59	0.55	43.3	3.64
210	3.0	15.6	5.0	2.19	1.24	1.15	75.6	6.49
350	3.0	10.4	5.0	2.71	2.39	2.27	84.7	13.97
Mean	3.0	10.4	4.9	2.12	1.41	1.32	67.9	8.03

[a]Limited by grid spacing.
[b]All negative streamers are assumed to eventually die.

Figure 8. Temporal evolution of (a) current and (b) power density in different leader channel sections due to a single step for which the characteristics of final link and positive part of space leader link are presented in Fig. 7. Green dashed lines in figures (a) show the exact value of feeding current, which was 214 A (rounded off value of 210 A is given in Fig. 7). 3D distances between the center of each channel section and the newly-formed leader tip are, from bottom to top, 8, 18, 30, 70, 132, and 221 m. The panels labeled "8 m" are the same as the corresponding panels in Fig. 7(I). Note different vertical scales used at different distances from the tip (except for current at 132 and 221 m).

Qi et al. [2016] observed three scenarios of space leader development: the space leader fails to make connection to the primary leader channel and eventually dies out (scenario A), the space stem develops into a space leader and connects to the primary leader tip or its lateral surface via a low luminosity region (scenario B), the space stem develops into a space leader, which connects to the primary leader channel forming a new step (scenario C). Scenario B was also described by *Edens et al.* [2014], who presented photographic records of steps in a cloud-to-air negative leader, and scenario C was observed by *Hill et al.* [2011]. All three scenarios introduced by *Qi et al.* [2016] were reproduced in our simulations.

Our simulations show that negative leader branches can die out. Despite the high conductivity of the leader channel, its peripheral sections (side branches) may disappear, with probability given by (12), after they become incapable of emanating new negative streamers. Once a negative leader branch starts decaying, it is usually chocked by the space charge of its own corona sheath, and can hardly recover and become active again. Indeed, the leader channel corona sheath charge reduces the electric field strength inside the sheath, which suppresses the growth of space leaders in its interior, so that they cannot reach the core of the branch and facilitate its extension. Once the branch dies out, space streamers / leaders continue to appear and die out at the periphery of the space-charge region left by that branch. This process ends only when the electric field becomes insufficient to support space streamer / leader initiation and development. Similar processes take place during the negative corona streamer burst at the end of step-formation process, when the newly formed negative leader tip abruptly emanates numerous negative streamers, whose charge reduces the electric field ahead of the leader tip. In what follows, if the negative leader branch "stays alive" long enough (cools slow enough) it may extend via a connection with a space leader; otherwise it progressively decays, until the entire branch disappears.

The main parameter determining the overall negative leader morphology in our model is the magnitude of the feeding current I_0. It's clear from Figures 5 and 6 that a higher feeding current results in more numerous leader branches. Specifically, the leader with the feeding current of 100 A has a single channel, while the leaders with 210- and 350-A feeding currents have two major branches at the end of simulation. Thus, the average current of a single leader branch is expected to be about 100-150 A. For a higher feeding current the leader channel growth direction becomes less sensitive to the background (vertical in our case) electric field strength and is largely determined by the field of charges near the tip. Because of this, leaders with the feeding currents of 210 and 350 A have more pronounced horizontal extent compared to the leader with the feeding current of 100 A. It follows from Tables 2-5 that most of the parameters of individual leader branches with the feeding currents of 100, 210, and 350 A are quite similar. These observations suggest that for a higher rate of charge supply to the leader channel there is a tendency for leader branching, with individual branches repelling each other, while the total number of major branches is limited by the minimum current (100 A or so) required to keep the branch alive.

DISCUSSION

A critical feature of our model is the polarity asymmetry (see Appendix A); that is, different initiation and propagation threshold fields for positive and negative streamers. Our simulation results would not be in good agreement with the experimental data for lightning without this feature. Although the initiation field for positive streamers $E_{ith}^{+} = 1.34$ MV/m exceeds the propagation field $E_{pth}^{-} = 0.62$ MV/m for negative ones, for the field (1.43 MV/m) at which the probability of occurrence of a new floating (positive) channel is equal to 50% the probability of existing negative channel extension is only 37% (see Fig. 3, red and green curves). As a result, at that field, it is easier to create a positive streamer originating from the space stem than to maintain the development of negative streamers from the primary leader channel tip. Thus, the main role in the step formation process is played by positive streamers originating from the space stem / leader, as the experimental data for long negative sparks suggest [e.g., *Bazelyan and Raizer*, 2000].
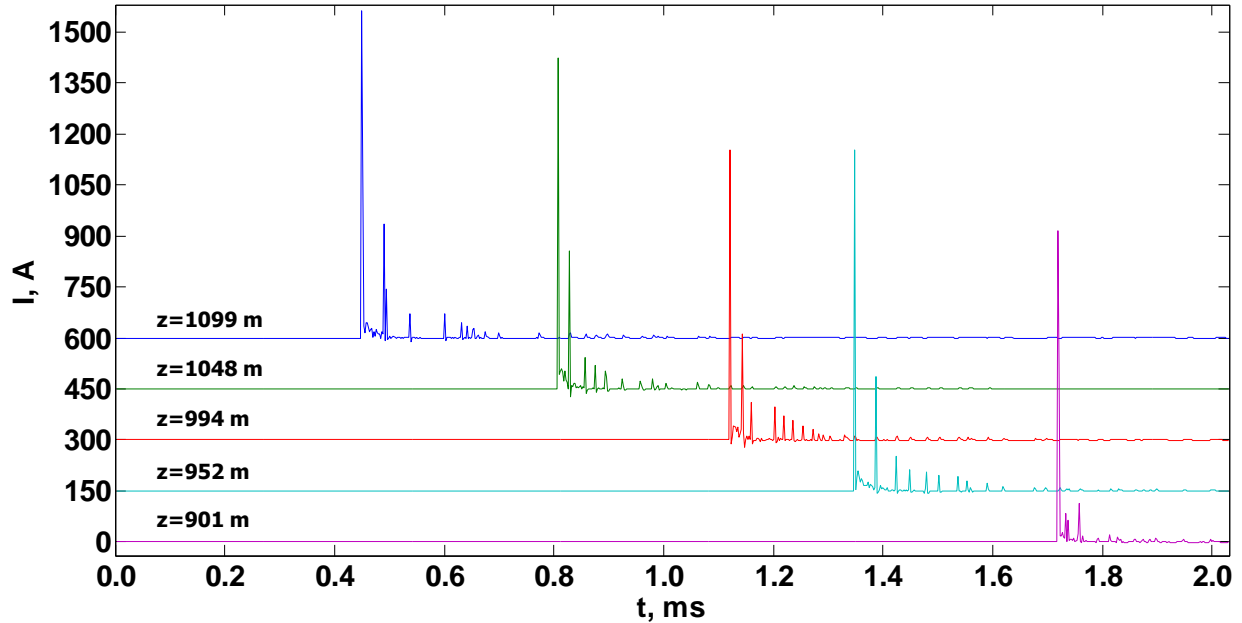
Another important feature of the model is the distinction between streamer-like and leader-like links based on their conductivity. The conductivity of streamer formations is expected to be of the order of 10^{-6}-10^{-5} S/m, while the mature-leader channel conductivity can be as high as 10^{4} S/m. We have chosen the lowest streamer conductivity to be 10^{-5} S/m and the threshold conductivity for streamer-to-leader transition (referred to the physical channel radius) to be 1 S/m. As noted in section 2.4, changing the threshold conductivity in the 0.1 to 10 S/m range does not lead to significant changes in our modeling results.

We now discuss the difference between positive and negative leader streamer zones. While the positive streamer zone usually appears to be uniform and developing continuously, the negative one is highly structured and transient [*Gorin and Skilev*, 1976]. At the final stage of the step formation process, it briefly exists in the form of intense corona streamer burst from the newly formed negative leader tip. Although in this study we don't describe in detail the negative streamer zone evolution, our model can reproduce all the salient features of this process. Since the model link length ranges from $a = 3$ m to $\sqrt{3}a = 5.2$ m, which could be smaller than the extent of negative streamer zone in lightning leader (see, for example, *Petersen and Beasley*, [2013]), the simulated negative streamer burst proceeds in several stages, as described next. At each subsequent model time step, newly-formed negative streamer links emerge from the tips of previously created ones, pushing negative charge farther and farther away from the primary leader channel tip. This relay-type process ends when the electric field becomes too low to support further propagation of negative streamers. Thus, the extent of the negative streamer corona is determined by the electric field in the vicinity of the negative leader tip. The negative streamer zone (corona streamer burst) doesn't strongly affect the charge transport, because its conductivity in the model is limited to 1 S/m (≤ 1 S/m), and because negative streamer links are quickly overlapped by positive streamer / leader links originating from space stems, whose conductivity growth is not capped in our model. Eventually, negative streamer links die out, leaving negative space charge behind, this charge being responsible for the shielding of the negative leader tip. Recall that we do not consider the possible motion of space stems in the present model.

As noted above, the leader channel is composed of a thin, highly-conducted core surrounded by a much larger, low conductivity sheath. Although it's known that the leader channel sheath originates from both the streamer zone developing from the leader tip and radial streamer corona from the lateral surface of the narrow leader channel core, our model accounts only for the former source of the sheath charge. Specifically, the leader channel corona sheath in the model forms from the space charge, which remains frozen at the grid nodes after the decay (extinction) of peripheral channels. The radial corona from the core was studied in detail by *Maslowsky and Rakov* [2006]. In our model, decayed links, contributing space charge to the leader channel corona sheath, are predominantly negative streamers growing from the leader channel tip and other nodes in its immediate vicinity. Note that the grid spacing of 3 m that we use in this study is insufficient to separate charges in the channel core from those in the channel sheath. To simulate the radial corona from the leader channel core one needs to calculate the electric field at its surface. Within the framework of our model, the electric field can be calculated only between a pair of nodes and has nothing to do with the radial electric field at the lateral surface of the leader channel core, which is extremely narrow (has radius of the order of a millimeter) compared with the model grid spacing (3 m). The issue of relative contributions of the two mechanisms to the formation of leader channel corona sheath can be solved only by accounting for subgrid effects and is a subject of a future research. A numerical model of corona discharge on horizontal conductors was recently developed by *Thang et al.* [2012].

Fig. 9 shows the time variation of transient current flowing through the 5 primary negative leader channel nodes located at 1099, 1048, 994, 952, and 901 m above the ground, for the event with feeding current of 100 A. Those nodes correspond to positions of negative leader tips formed at 0.37, 0.81, 1.12, 1.35, and 1.72 ms, respectively. The term "transient" means that this current is associated only with the charge variation occurring at specified nodes with the effect of feeding current removed. Note that the positive sign of the current corresponds to the upward motion of positive charge or the downward motion of negative charge (regardless of whether the charge of given sign enters or leaves the node), which is expected for descending negative leaders. The initial large current pulse at each height is associated with negative charge rapidly injected from the primary channel into the newly-formed leader tip (or positive charge of the space leader injected into the previously existed leader channel), as a result of the step formation process. This charge injection is also reflected in peaks (rapid fluctuations) in the vertical distribution of the line charge density in the negative leader channel sheath (see Fig. 5). The first large current pulse is followed by a sequence of smaller pulses associated with leader steps occurring later at lower heights and causing positive charge to travel up along the leader channel. The later (smaller) positive pulses correspond to progressively more distant (lower-altitude) leader steps. Fig. 9 is qualitatively similar to the dart-stepped leader luminosity profiles seen in Fig. 6 of *Wang et al.* [1999] and *Chen et al.* [1999]. Note that the current pulses associated with steps can significantly exceed the feeding current (100 A). This is a result of large electric fields (about 1-2 MV/m) between the tips of space and primary leaders at the beginning of the step-formation process, which rapidly reduce to the typical leader channel internal field value of about 10 kV/m. This electric field reduction takes as short as about 0.1 μs (see Fig. 7), and,

hence, requires a very high electric current. It's important to note that the feeding current is responsible only for the magnitude of the negative charge injected in the simulation domain at each model time step and is not directly related to currents in individual branches belonging to the primary negative leader.
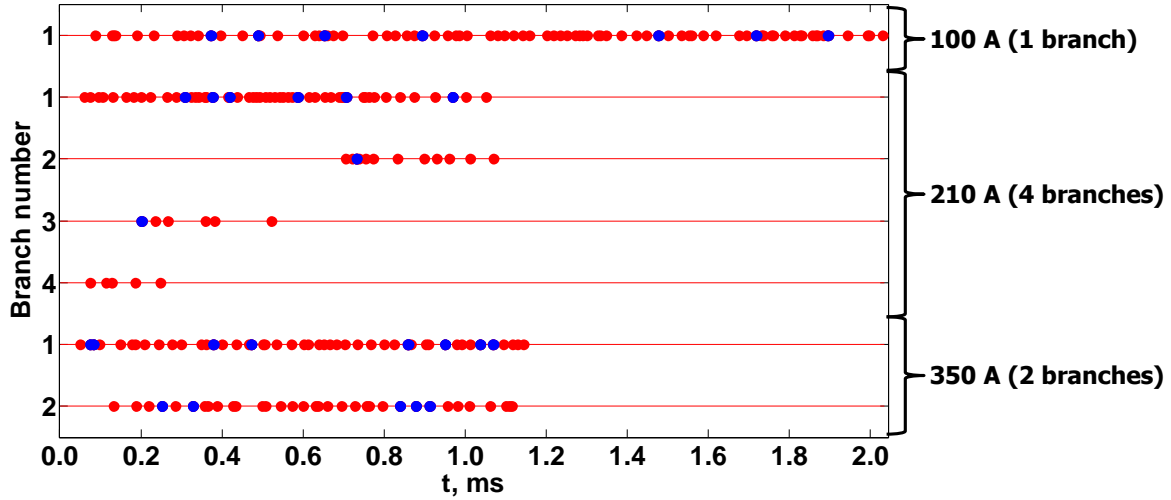

Figure 9. Transient leader current vs. time waveforms at different heights, 901, 952, 994, 1048, and 1099 m above the ground, corresponding to five negative leader tip positions, for the feeding current of 100 A (the event shown in Figs. 5a and 6(I)). Plots for 952, 994, 1048, and 1099 m are shifted up by 150, 300, 450, and 600 A, respectively, for improved viewing. The positive sign of the current corresponds to upward motion of positive or downward motion of negative charge, expected for descending negative leaders.

Fig. 10 shows the occurrence times of individual steps for all the branches of each of the three simulated leaders. The more than 2 orders of magnitude variation in the interstep time intervals (0.53-140.2 µs) predicted by the model is related to the fact that the steps can occur in multiple competing branches and are clustered in groups separated by relatively long time intervals, rather than being more or less equally spaced, as would be expected for a single-channel leader. Note that numerous quickly dying short branches with the lifetime of the order of tens of microseconds and the length of about ten meters (which are shown in grey in Figs. 5 and 6(I)) also participate in the competition and influence interstep intervals, which is especially evident for the leader with the feeding current of 100 A. That leader created only one main channel and about 30 short-leaved branches.

Note that such step parameters as the transferred charge, current peak, and final channel conductivity vary significantly for different steps. They are mainly determined by the local electric field configuration at the moment of connection of space leader to the primary leader channel. It's seen from Table 4 that the final conductivities of the final bridging links between the

space-leader and primary-leader channels are about twice higher for the feeding current of 100 A than for feeding currents of 210 and 350 A. This is probably because of relatively small number of space streamers / leaders for the relatively low feeding current of 100 A, which results in a less significant electric field reduction along the bridging streamer link and, as a consequence, higher final conductivity of that link. In contrast, for higher feeding currents, there is a larger number (see Table 5) of space streamers / leaders, which more effectively relax the electric field in the vicinity of the negative leader tip, leading to a smaller final conductivity of the bridging link. As each conducting link results in a decrease of electric field between the pair of nodes it bridges, a denser network of conducting links, which forms for higher feeding currents, means a lower electric field inside the volume occupied by that network.

Figure 10. Times of step occurrence in different branches of the 3 negative leaders shown in Figs. 5 and 6. Steps which are resolvable in time within the 3.33 μs time step are shown in red, while irresolvable ones are shown in blue. Feeding current and number of branches for each of the 3 leaders are given on the right.

One of the main results of this study is the finding that the occurrence of space stems and, hence, space leaders takes place under the influence of the electric field enhancement by the negative charge injected into the space ahead of the leader tip by the negative corona streamer burst at the end of the preceding step formation process. Numerical estimates show that, during the discharge development process, the electric field at the position of prospective space stem increases by approximately two orders of magnitude (in comparison with the background value) and is likely to exceed the threshold field $E_{ith}^{+} = 1.34$ MV/m in our model.

It is worth noting that the results obtained in this study are significantly influenced not only by the choice of the model input parameters, the most influential of which are the threshold fields and the grid spacing, but also by relations (8) and (9), describing the channel conductivity evolution, and relation (12) specifying the probability of channel decay. Those relations are somewhat subjective and tuned to achieve the expected results, which is unavoidable because the complexity of modeling of the electrical discharge development inevitably requires its parameterization. Clearly, there is a need for further experimental and theoretical studies to

develop more accurate parameterizations. On the other hand, the proposed approach is useful in determining the ranges of model parameters, which allow one to satisfactorily describe the observed features of the negative lightning stepped leader development.

CONCLUSION

A numerical model with unprecedentedly small grid spacing of 3 m was applied to studying the progression of negative lightning stepped leader. The model takes into account the difference between the initiation and propagation fields and, for the first time, employs different field thresholds for positive and negative streamers. This allows simulation of all stages of the stepping process, including the appearance of space stems inside and in the immediate vicinity of negative-leader streamer zone (corona streamer burst) and transformation of some of them into space streamers / leaders, which can extend biderectionally and connect to the primary leader channel, facilitating its stepwise extension. It appears that space stems occur as a result of electric field intensification by the space charge rapidly pushed into the space ahead of the newly-formed leader tip by the intense negative corona streamer burst, which completes the preceding step-formation process. A formal criterion for the streamer-to-leader transition in terms of channel conductivity was introduced and used, among other things, in order to facilitate identification of the final streamer link bridging the space and primary leader channels. Morphology and dynamics of simulated negative leaders are in good agreement with the results of recent observations of lightning stepped and dart-stepped leaders obtained using high-speed video cameras [*Hill et al*, 2011; *Petersen and Beasley*, 2013; *Tran et al.*, 2014; *Gamerota et al.*, 2014; *Lu et al*, 2016; *Qi et al*, 2016; *Jiang et al.*, 2017]. Further, the model-predicted electrical parameters are in line with the current knowledge on negative lightning leaders (see, for example, *Rakov and Uman* [2003, ch. 4] and *Nag and Rakov* [2016] and references therein).

APPENDIX A: POLARITY ASYMMETRY

All presently existing numerical models describing lightning discharge development (see, for example, [*Mansell*, 2002; *Tan et al.*, 2006; *Riousset et al.*, 2007; *Mansell et al.*, 2010; *Iudin and Davydenko*, 2015; *Iudin et al.*, 2015; *Davydenko and Iudin*, 2016; *Wang et al.*, 2016; *Iudin et al.*, 2017]) don't consider the difference in fields required for propagation of positive and negative streamers. This polarity asymmetry is well known from laboratory spark studies, which indicate that the fields in streamer zones of positive and negative leaders, which are approximately constant, differ by about a factor of 2 and are equal to about 5 and 10 kV/cm, respectively [*Raizer*, 2009, p. 596; *Gorin and Shkilev*, 1976]. It is reasonable to assume that the propagation fields for positive and negative streamers are close to the electric fields inside positive and negative leader streamer zones, respectively, and, hence, differ by a factor of 2 or so. This inference is in general agreement with the modeling result obtained by *Gallimberti et al.* [2002], who theoretically examined the energy gain and loss at the streamer front and found that the magnitudes of stability fields corresponding to the energetically stable streamer propagation are 5 and 7.5 kV/cm for positive and negative streamers, respectively.

The polarity asymmetry is related to the difference in direction in which electrons move relative to the streamer head of different polarity. In a positive streamer, electrons produced in the vicinity of its head move towards it, so the ionization tends to happen in a stronger field. The head of negative streamer pushes electrons away (to a lower field region), so that ionization takes place under less favorable conditions (see, for example, *Bazelyan and Raizer* [2000, p. 84]). In other words, a stronger field is required for negative streamer development, when electrons have to move to a lower field region. The effect can be also related to the role of low-mobility positive space charge, which is produced in the tails of electron avalanches and serves to either enhance (positive streamer) or oppose (negative streamer) the external field in the forward direction. Further discussion of reasons for polarity asymmetry can be found in works of *Williams* [2006] and *Kostinskiy et al.* [2017].

Observations show that the streamer zone of positive leader in laboratory consists of positive streamers only (see, for example, *Bazelyan and Raizer* [2000, Fig. 2.2]). Extension of positive leaders in laboratory is optically continuous, at least when the absolute humidity is lower than 10 g/m^3 or so and when the voltage impulse front is less than 1 ms or so (see *Kostinskiy et al.* [2017] and references therein). In lightning, both continuously moving and stepping positive leaders were observed (see *Rakov and Uman* [2003, p. 137] and references therein).

In contrast to positive leaders, the streamer zone of negative leader in long laboratory sparks and in lightning is complex and appears to consist of both negative and positive streamers [*Bazelyan and Raizer*, 2000, p. 85; *Gorin and Shkilev*, 1976; *Gamerota et al.*, 2014]. Further, negative leaders developing in virgin air are always stepped. During the step formation process, positive streamers extending from the space stem / space leader toward the primary leader channel come in contact with negative streamers emanated from the primary leader tip. There are also negative streamers extending from the space stem / leader in the forward (the same as the overall leader extension) direction. When the positive end of space leader makes connection with the primary leader channel, the high potential of negative leader tip is rapidly transferred to the lower extremity of the space leader. This causes a powerful burst of negative corona streamers from the newly formed negative leader tip that was recently studied by *Kostinskiy et al.* [2017]. The streamer burst apparently creates conditions in which new space stems are born. Some of them evolve into new steps, with typical interstep time intervals being some tens of μs.

REFERENCES

1. Bazelyan, J. M., and Y. P. Raizer (1998), *Spark Discharge*, CRC Press, Boca Raton, New York.
2. Bazelyan, E. M., and Y. P. Raizer (2000), *Lightning Physics and Lightning Protection*, Institute of Physics Publishing, Bristol, Philadelphia.
3. Cooray V., and L. Arevalo (2017), Modeling the stepping process of negative lightning stepped leaders, *Atmosphere*, 8, 245, doi:10.3390/atmos8120245.
4. Chen, M., N. Takagi, T. Watanabe, D. Wang, Z.-I. Kawasaki, and X. Liu (1999), Spatial and temporal properties of optical radiation produced by stepped leaders, *J. Geophys. Res.*, 104, 27,573–27,584, doi:10.1029/1999JD900846.

5. Davydenko, S. S., and D. I. Iudin (2016), Fractal model of a compact intracloud discharge. II. Unique features of electromagnetic emission, *Radiophys. Quantum Electron.*, 59(7), 560-575, doi: 10.1007/s11141-016-9723-5.

6. Dulzon, A. A., V. V. Lopatin, M. D. Noskov, and O. L. Pleshkov (1999), Modelling the development of the stepped leader of a lightning discharge, *Tech. Phys.*, 44(4), 394-398. (Translated from Russian 1999 *Zh. Tech. Fiz.*, 69(4), 48-53).

7. Edens, H. E., K. B. Eack, W. Rison, and S. J. Hunyady (2014), Photographic observations of streamers and steps in a cloud-to-air negative leader, Geophys. Res. Lett., 41, 1336–1342, doi:10.1002/2013GL059180.

8. Gallimberti, I., G. Bacchiega, A. Bondiou-Clergerie, and P. Lalande (2002), Fundamental processes in long air gap discharges, *CR Phys.*, 3(10), 1335-1359.

9. Gamerota, W. R., V. P. Idone, M. A. Uman, T. Ngin, J. T. Pilkey, and D. M. Jordan (2014), Dart-stepped-leader step formation in triggered lightning, *Geophys. Res. Lett.*, 41, 2204–2211, doi:10.1002/2014GL059627.

10. Gorin, B. N. and A. V. Shkilev (1976), The development of electrical discharge in long gaps rod-plane with a negative voltage pulse, *Elektrichestvo* (in Russian), 6, 31–39.

11. Heckman, S. J. and E. R. Williams (1989), Corona envelops and lightning currents, *J. Geophys. Res.*, 94, D11, 13,287-13,294, doi: 10.1029/JD094iD11p13287.

12. Hill J. D., M.A. Uman, and D.M. Jordan (2011), High-speed video observations of a lightning stepped leader, J. Geophys. Res., 116, D16117, doi:10.1029/2011JD015818.

13. Hill, J. D., M. A. Uman, D. M. Jordan, T. Ngin, W. R. Gamerota, J. Pilkey, and J. Caicedo (2016), The attachment process of rocket-triggered lightning dart-stepped leaders, *J. Geophys. Res. Atmos.*, 121, 853–871, doi:10.1002/2015JD024269.

14. Iudin, D. I., and S. S. Davydenko (2015), Fractal model of a compact intracloud discharge. I. Features of the structure and evolution, Radiophys. Quantum Electron., 58(7), 477-496, doi:10.1007/s11141-015-9621-2.

15. Iudin, D. I., F. D. Iudin, and M. Hayakawa (2015), Modeling of the intracloud lightning discharge radio emission, *Radiophys. and Quantum Electron.*, 58(3), 173-184, doi: 10.1007/s11141-015-9591-4.

16. Iudin, D. I., V. A. Rakov, E. A. Mareev, F. D. Iudin, A. A. Syssoev, and S. S. Davydenko (2017), Advanced numerical model of lightning development: Application to studying the role of LPCR in determining lightning type, *J. Geophys. Res. Atmos.*, 122, doi:10.1002/2016JD026261.

17. Jiang, R., X. Qie, H. Zhang, M. Liu, Z. Sun, G. Lu, Z. Wang, and Y. Wang (2017), Channel branching and zigzagging in negative cloud-to-ground lightning, *Sci. Rep.*, 7(3457), 1-8, doi:10.1038/s41598-017-03686-w.

18. Kostinskiy, A. Y., V. S. Syssoev, N. A. Bogatov, E. A. Mareev, M. G. Andreev, M. U. Bulatov, L. M. Makal'sky, D. I. Sukharevsky, and V. A. Rakov (2016), Observations of the connection of positive and negative leaders in meter-scale electric discharges generated by clouds of negatively charged water droplets, *J. Geophys. Res. Atmos.*, 121, 9756–9766, doi:10.1002/2016JD025079.

19. Kostinskiy, A. Yu., V. S. Syssoev, N. A. Bogatov, E. A.Mareev, M. G. Andreev, M. U. Bulatov, D. I. Sukharevsky, and V. A. Rakov (2017), Abrupt Elongation (Stepping) of Negative and Positive Leaders Culminating in an Intense Corona Streamer Burst: Observations in Long Sparks and Implications for Lightning, *J. Geophys. Res. Atmos.*, in review.

20. Lu, W., Q. Qi, Y. Ma, et al. (2016), Two basic leader connection scenarios observed in negative lightning attachment process, *IET Generation, Transmission and Distribution*, Special Issue: Lightning and Lightning Protection, 1-7, doi: 10.1049/hve.2016.0002.

21. MacGorman, D. R., and W. D. Rust (1998), The Electrical Nature of Thunderstorms, Oxford University Press, New York.

22. Mansell, E. R. (2002), Simulated three-dimensional branched lightning in a numerical thunderstorm model, *J. Geophys. Res.*, 107, D9, ACL 2-1-ACL 2-12, doi:10.1029/2000JD000244.

23. Mansell, E. R., C.L. Ziegler, E.C. Bruning (2010), Simulated Electrification of a Small Thunderstorm with Two-Moment Bulk Microphysics, *J. Atmos. Sci.*, 67, 171-194, doi: 10.1175/2009JAS2965.1.

24. Nag, A., and V. A. Rakov (2016), A unified engineering model of the first stroke in downward negative lightning, *J. Geophys. Res. Atmos.*, 121, 2188–2204, doi:10.1002/2015JD023777.

25. Ortega, P., P. Domens, A. Gibert, B. Hutzler, and G. Riquel (1994), Performance of a 16.7 m air rod-plane gap under a negative switching impulse, *J. Phys. D Appl. Phys.*, 27, 2379-2387.

26. Petersen, D. A., and W.H. Beasley (2013), High-speed video observations of a natural negative stepped leader and subsequent dart-stepped leader, *J. Geophys. Res. Atmos.*, 118, 12,110-12,119, doi:10.1002/2013JD019910.

27. Qi Q., W. Lua, and Y. Ma, L. Chen, Y. Zhang, and V. A. Rakov (2016), High-speed video observations of the fine structure of a natural negative stepped leader at close distance, *Atmos. Res.*, 178-179, 260-267, doi: 10.1016/j.atmosres.2016.03.027.

28. Raizer, Y. P. (2009), *Gas Discharge Physics* (in Russian), Intellect, Dolgoprudny.

29. Rakov, V. A., and M. A. Uman (2003), *Lightning: Physics and Effects*, Cambridge Univ. Press, New York.

30. Rees, T., P. Ortega, A. Gibert, P. Domens, and P. Pignolet (1995), An experimental study of negative discharge in a 1.3 m point-plane air gap: the function of the space stem in the propagation mechanism, *J. Phys. D Appl. Phys.*, 28, 2306-2313.

31. Riousset, J. A., V. P. Pasko, P. R. Krehbiel, R. J. Thomas, and W. Rison (2007), Three-dimensional fractal modeling of intracloud lightning discharge in a New Mexico thunderstorm and comparison with lightning mapping observations, *J. Geophys. Res.*, 112, D15203, doi:10.1029/2006JD007621.

32. Rompe, R., and W. Weizel (1944), Uber des Toeplersche Funkengesetz (on the Toepler spark theory), *Zt. Phys.*, 122, 636-639, doi:10.1007/BF01330625.

33. Tan, Y., S. Tao, and B. Zhu (2006), Fine-resolution simulation of the channel structures and propagation features of intracloud lightning, *Geophys. Res. Lett.*, 33, L09809, doi:10.1029/2005GL025523.

34. Thang, T. H.,Y. Baba, N. Nagaoka, A. Ametani, J. Takami, S. Okabe, and V. A. Rakov (2012), A Simplified model of corona discharge on overhead wire for FDTD computations, *IEEE T ELECTROMAGN C*, Vol. 54, No. 3, 585-593, doi:10.1109/TEMC.2011.2172688.

35. Tran, M. D. and V. A. Rakov (2017), A study of the ground-attachment process in natural lightning with emphasis on its breakthrough phase, *Sci. Rep.*, 7: 15761, 1-13, doi:10.1038/s41598-017-14842-7.

36. Tran, M. D., V. A. Rakov, S. Mallick (2014), A negative cloud-to-ground flash showing a number of new and rarely observed features, *Geophys. Res. Lett.*, 41, 6523–6529, doi:10.1002/2014GL061169.

37. van der Velde, O. A., J. Montanyà (2013), Asymmetries in bidirectional leader development of lightning flashes, *J. Geophys. Res. Atmos.*, 118, 13,504-13,519, doi:10.1002/2013JD020257.

38. Wang, D., N. Takagi, T. Watanabe, V. A. Rakov, and M. A. Uman (1999), Observed leader and return-stroke propagation characteristics in the bottom 400 m of a rocket-triggered lightning channel, *J. Geophys. Res.*, Vol. 104, No D12, 14,369-14,376.

39. Wang, H., F. Guo, T. Zhao, M. Qin, and L. Zhang (2016), A numerical study of the positive cloud-to-ground flash from the forward flank of normal polarity thunderstorm, *Atmos. Res.*, 169, 183-190.

40. Williams, E. R. (2006), Problems in lightning physics - the role of polarity asymmetry, *Plasma Sources Science and Technology*, 15, S91.

41. Wu, T., S. Yoshida, Y. Akiyama, M. Stock, T. Ushio, and Z. Kawasaki (2015), Preliminary breakdown of intracloud lightning: Initiation altitude, propagation speed, pulse train characteristics, and step length estimation, *J. Geophys. Res. Atmos.*, 120, 1-16, doi:10.1002/2015JD023546.

42. Zhang, X., Y. Zhu, S. Gu, and J. He (2017), Dynamics of branching of negative downward lightning leaders, *Appl. Phys. Lett.*, 111, 224101, doi:10.1063/1.5010714.